LETTER

doi:10.1038/nature22334

A Wnt-producing niche drives proliferative potential and progression in lung adenocarcinoma

Tuomas Tammela[1], Francisco J. Sanchez-Rivera[1], Naniye Malli Cetinbas[1], Katherine Wu[1], Nikhil S. Joshi[1], Katja Helenius[1], Yoona Park[1], Roxana Azimi[1], Natanya R. Kerper[1], R. Alexander Wesselhoeft[1], Xin Gu[1], Leah Schmidt[1], Milton Cornwall-Brady[1], Ömer H. Yilmaz[1], Wen Xue[1,2], Pekka Katajisto[3,4], Arjun Bhutkar[1] & Tyler Jacks[1,5]

The heterogeneity of cellular states in cancer has been linked to drug resistance, cancer progression and the presence of cancer cells with properties of normal tissue stem cells[1,2]. Secreted Wnt signals maintain stem cells in various epithelial tissues, including in lung development and regeneration[3–5]. Here we show that mouse and human lung adenocarcinomas display hierarchical features with two distinct subpopulations, one with high Wnt signalling activity and another forming a niche that provides the Wnt ligand. The Wnt responder cells showed increased tumour propagation ability, suggesting that these cells have features of normal tissue stem cells. Genetic perturbation of Wnt production or signalling suppressed tumour progression. Small-molecule inhibitors targeting essential posttranslational modification of Wnt reduced tumour growth and markedly decreased the proliferative potential of lung cancer cells, leading to improved survival of tumour-bearing mice. These results indicate that strategies for disrupting pathways that maintain stem-like and niche cell phenotypes can translate into effective anti-cancer therapies.

Stem cells are defined by their capacity to self-renew while also producing differentiated cells. The decision to divide or differentiate is primarily controlled by extrinsic signalling factors, which, together with the cells that produce them, form a niche with a local range of action capable of supporting a limited number of stem cells. Among the niche signals that promote stem-cell phenotypes, secreted Wnt proteins are notable owing to their function in multiple epithelial stem cell compartments[3]. Wnt growth factors are palmitoylated in cells that produce them by the membrane-bound O-acyltransferase porcupine (encoded by *Porcn* in mice)[3]. This posttranslational modification is essential for Wnt secretion and binding to frizzled family receptors[3]. Wnt binds frizzled, promoting the stabilization, nuclear translocation and transcriptional activity of β-catenin through its interaction with T-cell factor (TCF) family transcription factors. Recently, R-spondin (Rspo) growth factors were found to amplify Wnt signalling by engaging leucine-rich repeat-containing G-protein-coupled receptor (Lgr)4, Lgr5 and Lgr6 (ref. 6). Lgr5 marks stem cells in multiple epithelial tissues and in intestinal adenomas[3,6–8]. Stem-like cells have recently been described in autochthonous mouse tumour models[7,9,10] and in tumour transplants[11–13], but evidence for the existence of stem-like cells and particularly their niche in advanced solid tumours *in situ* has been limited[14].

Lung adenocarcinoma (LUAD) is a leading cause of death globally. Tumours driven by oncogenic KRAS account for approximately 30% of LUAD and effective chemotherapies against these tumours are lacking[15]. Wnt signalling is essential for the initiation and maintenance of Braf-driven lung adenomas in mice[16], and forced activation of the pathway promotes progression of Kras or Braf mutant lung tumours[16,17]. LUAD in humans, in particular tumour metastasis, is frequently associated with increased expression of Wnt-pathway-activating genes and downregulation of negative regulators of this pathway[18,19].

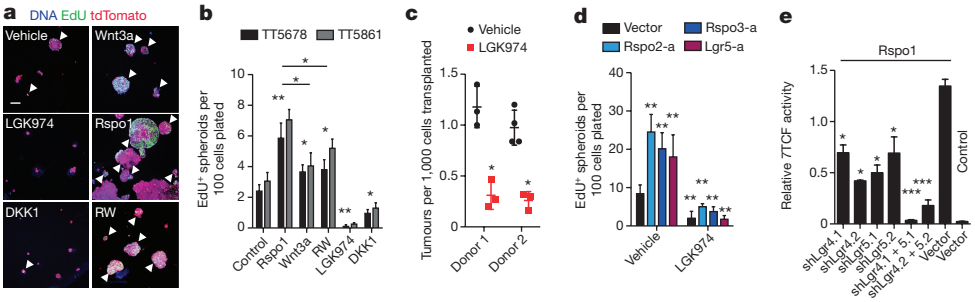

Figure 1 | Ligand-dependent Wnt signalling sustains proliferative potential in lung adenocarcinoma. a, 3D cultures of sorted tdTomato$^+$ (red) primary mouse KPT LUAD cells 14 days after plating. Proliferating (EdU$^+$) cells (green, arrowheads). RW, combination of Rspo1 and Wnt3a. Scale bar, 100 μm. **b**, Quantification of tumour spheroids containing EdU$^+$ cells from two mice (TT5678 and TT5861). $n = 8$ wells per condition. **c**, Quantification of KPT LUAD primary transplant tumours in recipient mouse lungs treated with LGK974 or vehicle for eight weeks. **d**, Quantification of tumour spheroids containing EdU$^+$ cells ten days after plating. Rspo2-a, Rspo3-a and Lgr5-a refer to cells expressing CRISPR-activator (SAM) components driving expression of the indicated gene. $n = 8$ wells per condition. **e**, Wnt pathway activity measured by the Topflash assay in cultured KP LUAD cells stably expressing shRNAs targeting *Lgr4*, *Lgr5*, both *Lgr4* and *Lgr5* or a vector control. $n = 3$ technical replicates per condition, experiment was repeated four times. Data are mean ± s.d.; two-way ANOVA (**b**, **d**, **e**) or Student's *t*-test (**c**); $*P < 0.05$; $**P < 0.01$; $***P < 0.001$ compared to control, except in **d**, where the LGK974 group is compared to the same CRISPR-activator line, and in **e** where the comparison is to Rspo1 stimulation.

[1]David H. Koch Institute for Integrative Cancer Research, Massachusetts Institute of Technology, Cambridge, Massachusetts 02142, USA. [2]RNA Therapeutics Institute, Program in Molecular Medicine, and Department of Molecular, Cell and Cancer Biology, University of Massachusetts Medical School, Worcester, Massachusetts 01605, USA. [3]Institute of Biotechnology, University of Helsinki, 00014 Helsinki, Finland. [4]Department of Biosciences and Nutrition, Karolinska Institutet, 14183 Stockholm, Sweden. [5]Howard Hughes Medical Institute, Massachusetts Institute of Technology, Cambridge, Massachusetts 02139, USA.

We isolated tdTomato$^+$ primary cancer cells from autochthonous *Kras*$^{G12D/+}$;*Trp53*$^{\Delta/\Delta}$;*Rosa26*$^{tdTomato/+}$ (KPT) mouse LUAD, and established low-density three-dimensional (3D) organotypic tumour spheroid cultures. 2.7% (±0.5% (mean ± s.d.)) of the cells gave rise to persistently proliferating spheroids (Fig. 1a, b), suggesting that cells capable of self-renewal comprise a small minority of the tumour. Recombinant Wnt3a, Rspo1 or their combination increased the absolute number and ratio of primary mouse KPT LUAD spheroids that contained proliferating cells, and promoted overall cell proliferation (Fig. 1a, b and Extended Data Fig. 1a, b). Conversely, inhibition of ligand-driven Wnt signalling with the porcupine inhibitor LGK974 (ref. 20), short-hairpin RNA (shRNA) targeting *Porcn* or recombinant DKK1 (a Wnt antagonist[3]) suppressed proliferative capacity of primary LUAD cells in 3D spheroids (Fig. 1a, b and Extended Data Fig. 1a–f). Tumour formation by primary LUAD cells was markedly decreased upon orthotopic transplantation (genetically engineered mouse model-derived allograft, GEMM-DA) into recipient mice that were treated with LGK974 compared to control (Fig. 1c and Extended Data Fig. 1g). Collectively, these data indicate that KP LUAD cells display heterogeneity in their proliferative potential, which is maintained by Wnt signals produced by cancer cells.

Rspo1 alone was most potent in stimulating proliferation and expansion of KPT LUAD spheroids (Fig. 1a, b and Extended Data Fig. 1a), even though, as expected, the combination of recombinant Rspo1 and Wnt3a was most potent in activating the Wnt pathway (Extended Data Fig. 1e, h and Supplementary Information). We next used the CRISPR–Cas9-based synergistic activation mediator (SAM) system[21] to robustly drive expression of *Rspo2*, *Rspo3* or *Lgr5* in KP LUAD cells (Extended Data Fig. 1i–l). This increased their proliferation and induced Wnt target genes in 3D spheroid culture and both of these effects were suppressed by LGK974 (Fig. 1d and Extended Data Fig. 1m, n). Knockdown of both *Lgr4* and *Lgr5* was required to fully suppress R-spondin-driven Wnt pathway activation (Fig. 1e and Extended Data Fig. 2a–g), indicating that both Lgr4 and Lgr5 are R-spondin receptors in the KP LUAD model.

We next assessed whether the Wnt pathway is activated in autochthonous KP LUAD tumours *in vivo*. Using a luciferase or GFP-reporter gene driven by a synthetic β-catenin-sensitive 7TCF promoter, we observed Wnt-pathway activation in a subpopulation of cancer cells, particularly in large autochthonous KP tumours (Fig. 2a, b). In subcutaneous transplants of KP tumour lines, 7TCF promoter activity was suppressed by treatment with LGK974 (Extended Data Fig. 3a–c). Notably, we observed nuclear localization of β-catenin, a hallmark of activation of Wnt signalling, in a subpopulation of cancer cells, only in tumours that had progressed from adenoma to adenocarcinoma (Fig. 2c, d and Extended Data Fig. 3d).

We next performed porcupine immunostaining in tumour sections to identify cells that were able to produce Wnt in the LUAD tumours. Porcupine localized to cancer cells in close proximity to cells with nuclear β-catenin or expression of the Wnt target gene *Axin2* in autochthonous KP LUAD, although rare porcupine$^+$ macrophages were also detected, predominantly in peritumoural areas (Fig. 2c and Extended Data Fig. 3e–i). Furthermore, *Porcn* gene expression was significantly higher in adenocarcinomas compared to adenomas (Fig. 2e). Notably, we detected similar porcupine- or nuclear β-catenin-positive subpopulations and induction of *PORCN* expression in human LUAD (Fig. 2f and Extended Data Fig. 3j, k). These findings indicate that the Wnt pathway is activated in a subpopulation of lung adenocarcinoma cells in close proximity to porcupine$^+$ cells that are able to provide the Wnt signal. Porcupine localized to bronchiolar epithelium in the normal lung and was restricted to sites of high Wnt signalling and stem cell activity in the intestine and liver[3] (Extended Data Fig. 4a–e), suggesting that porcupine is specifically expressed in Wnt-producing cells in normal stem cell niches.

To test the functional requirement for porcupine expression in LUAD cells *in vivo*, we used CRISPR–Cas9 to inactivate *Porcn* specifically in

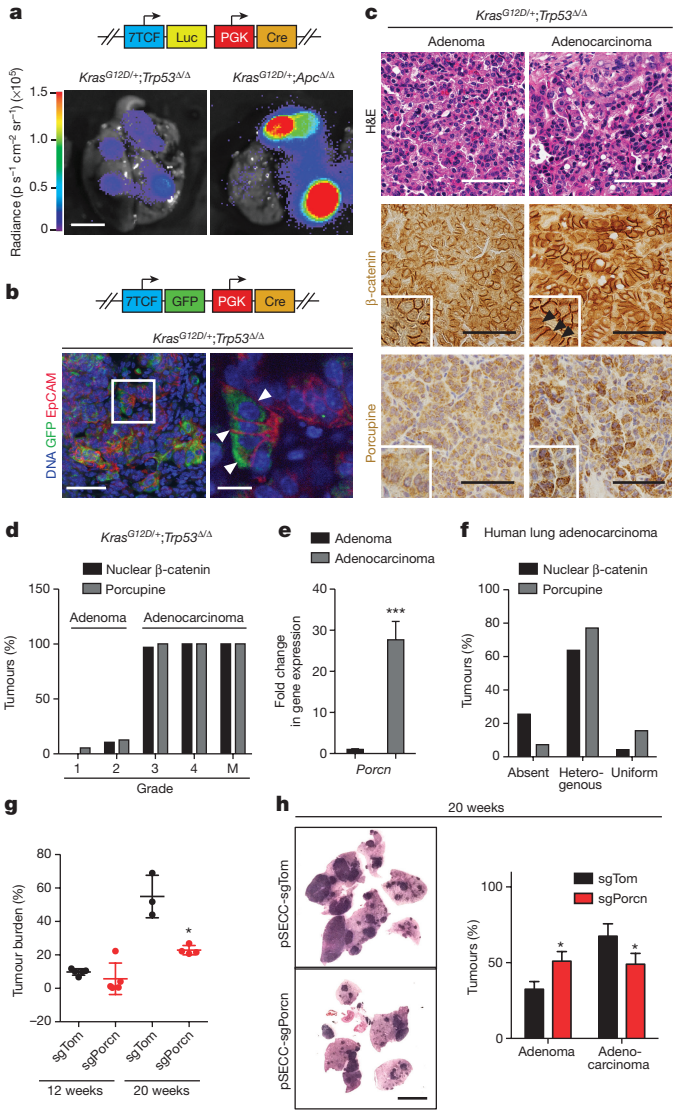

Figure 2 | Porcupine$^+$ cancer cells form a niche that drives Wnt signalling in lung adenocarcinoma. a, Bioluminescence in lungs of *Kras*$^{LSL\text{-}G12D/+}$;*Trp53*$^{flox/flox}$ (KP) or *Kras*$^{LSL\text{-}G12D/+}$;*Apc*$^{flox/flox}$ mice 20 weeks after intratracheal infection with the 7TCF::luciferase-PGK::Cre lentivirus (see schematic). **b**, GFP (green) and EpCAM (red) staining in KP LUAD tumours 20 weeks after infection with the 7TCF::GFP-PGK::Cre lentivirus (see schematic). Arrowheads indicate GFP$^+$ cells with 7TCF promoter activity. **c**, Haematoxylin and eosin (H&E), β-catenin or porcupine staining in KP adenomas or in adenocarcinomas. Note nuclear localization of β-catenin in adenocarcinomas (arrowheads). **d**, Percentage of tumours containing subpopulations of cells with porcupine expression or nuclear β-catenin per histological grade or in metastases (M). $n = 19$ grade 1, $n = 47$ grade 2, $n = 31$ grade 3 and $n = 11$ grade 4 tumours and $n = 6$ lymph node or thoracic wall metastases. **e**, Quantitative PCR analysis of *Porcn* gene expression in KP tumours at 9 weeks (adenomas) or 20 weeks (adenocarcinomas) after initiation. ***$P < 0.001$, $n = 16$. **f**, Percentage of human lung adenocarcinomas with absent, heterogenous or uniform porcupine expression or nuclear β-catenin. $n = 65$. **g**, Quantification of tumour burden in KP mice 12 or 20 weeks after infection with 25,000 transforming units of sgRNA-EFS-Cas92aCre (pSECC)–sgTom or pSECC–sgPorcn lentiviruses. **h**, Haematoxylin and eosin staining of KP LUAD-bearing lungs generated with pSECC–sgTom or pSECC–sgPorcn and quantification of the proportion of adenomas versus adenocarcinomas at 20 weeks following tumour initiation. Scale bars, 5 mm (**a**), 2 mm (**h**), 100 μm (**b** (left), **c**) and 10 μm (**b** (right)). Data are mean (**d**, **f**) or mean ± s.d. (**e**, **g**, **h**); *$P < 0.05$; Student's two-sided *t*-test (**e**, **g**, **h**).

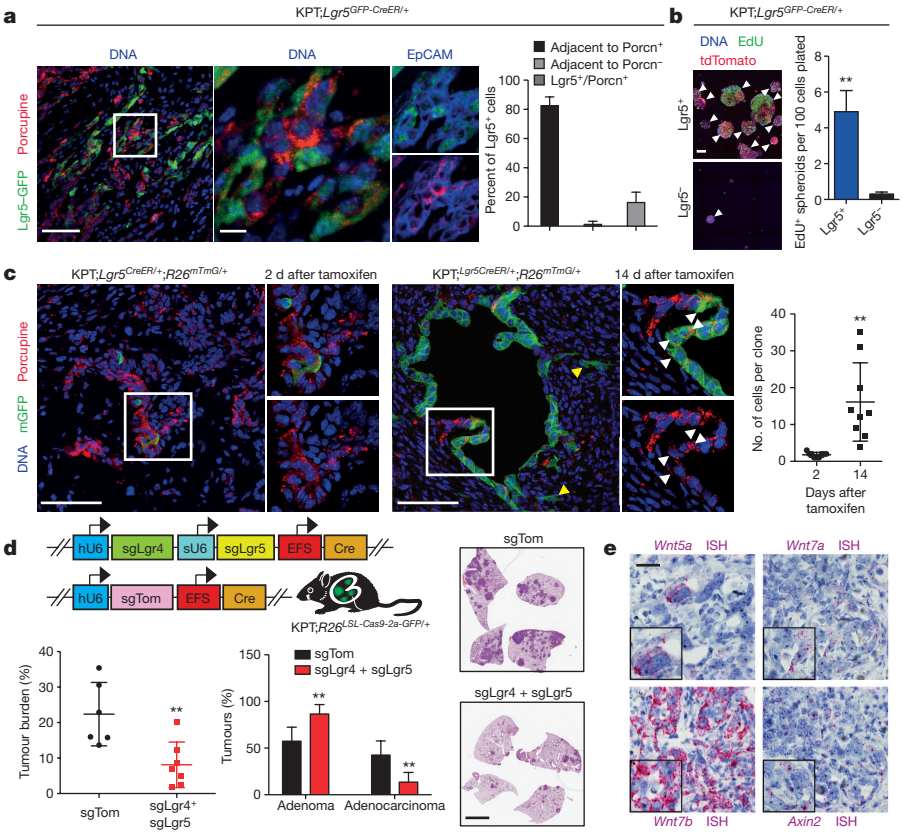

Figure 3 | Lgr5$^+$ lung adenocarcinoma cells display persistent proliferative potential. a, Immunostaining for GFP (green), porcupine (red) and EpCAM (blue) in a subcutaneous transplant of primary KP;*Lgr5*$^{GFP\text{-}CreER/+}$ LUAD cells three weeks after transplantation. Scale bars, 100 μm (left) and 10 μm (right). Quantification of the percentage of Lgr5$^+$ cells that are adjacent to porcupine$^+$ or porcupine$^-$ cells, or that are positive for both Lgr5 and porcupine in the transplants. $n = 6$ tumours. **b**, 3D culture of Lgr5$^+$ and Lgr5$^-$ KP LUAD cells. Quantification of primary spheroids containing EdU$^+$ cells (arrowheads). $n = 8$ wells per group. **c**, Lineage-tracing of KP;*Lgr5*$^{CreER/+}$;*Rosa26*$^{LSL\text{-}mTmG/+}$ LUAD cells in established subcutaneous primary transplants. Note migration of individual mGFP$^+$ cells (yellow arrowheads) away from clones derived from Lgr5$^+$ cells, and porcupine$^+$ progeny arising from Lgr5$^+$ cells (white arrowheads). $n = 9$ tumours per group. Quantification of average clone size at 2 (2 d) and 14 (14 d) days after tamoxifen administration. **d**, Quantification of tumour burden and proportion of adenomas and adenocarcinomas, and haematoxylin-eosin staining in KP;*Rosa26*$^{LSL\text{-}Cas9\text{-}2a\text{-}GFP/+}$ mice infected with the indicated lentiviral vectors. hU6, human U6 promoter; sU6, synthetic U6 promoter; EFS, minimal E1α promoter. $n = 6$ (sgTom), $n = 7$ (sgLgr4 + sgLgr5). **e**, mRNA ISH for the indicated transcripts (purple) in consecutive sections of a similar region of a KP lung adenocarcinoma. Scale bars, 2 mm (**d**) and 100 μm (**b**, **c**, **e**). Data are mean ± s.d.; $^*P < 0.05$, $^{**}P < 0.01$; Student's two-sided *t*-test (**a**–**d**).

the cancer cells of the KP LUAD model. Notably, targeting *Porcn* did not affect tumour grade or burden at 12 weeks after tumour initiation, when most tumours are still in the adenoma stage (Fig. 2g and Extended Data Fig. 5a). However, targeting *Porcn* reduced tumour burden and resulted in a shift to lower grade tumours at 20 weeks compared to control (Fig. 2g, h). Of note, of the 12 tumours that were graded as adenocarcinomas, 10 predominantly contained wild-type *Porcn* alleles or small non-frameshift mutations(Extended Data Fig. 5b, c). In 2 out of 12 of these tumours, in which substantial allelic fractions of frameshift mutations were detected, the tumours still maintained residual porcupine immunopositivity (data not shown). These data suggest that only tumours with at least a fraction of cells retaining functional *Porcn* were capable of progressing beyond adenomas.

Lgr5 is a Wnt target gene functionally involved in amplification of Wnt signalling and stem cell maintenance in multiple tissues[3,6]. When compared to adenomas, KP adenocarcinomas had an increased level of *Lgr5* transcripts, which localized to a subpopulation of adenocarcinoma cells (Extended Data Fig. 6a, b). *Lgr4* expression in KP LUAD tumours was more widespread compared to *Lgr5*, much like in normal intestinal crypts[6], but was enriched in the Lgr5$^+$ cells (Extended Data Fig. 6b–d). Furthermore, in GEMM-DAs established from KP LUAD tumours containing an *Lgr5*$^{GFP\text{-}CreER/+}$ reporter allele, the Lgr5$^+$ cells were localized in close proximity to porcupine$^+$ cancer cells (Fig. 3a). Sorted primary Lgr5$^+$ KP LUAD cells were more efficient at forming persistently proliferating spheroids *in vitro* and orthotopic KP LUAD GEMM-DA tumours *in vivo* than the Lgr5$^-$ cells (Fig. 3b and Extended Data Fig. 6e–g), suggesting that these cells have a high proliferative potential.

To investigate whether the Lgr5$^+$ cells also display stem-like properties *in situ* in established tumours, we established subcutaneous KP LUAD GEMM-DAs containing *Lgr5*^{CreER} and *Rosa26*^{mTmG} alleles, which allowed inducible labelling of the Lgr5$^+$ lineage in established tumours with membrane-associated GFP (mGFP) using tamoxifen. Single mGFP$^+$ cells were found two days after the tamoxifen pulse in porcupine$^+$ niches, whereas significant expansion of the Lgr5$^+$ clones was observed at 14 days after tamoxifen administration (Fig. 3c). The absolute number of clones did not change significantly over time (Extended Data Fig. 6h). Notably, the Lgr5$^+$ cells gave rise to porcupine$^+$ cells during the 14-day chase (Fig. 3c), indicating that the Lgr5$^+$ stem-like cells can give rise to their own niche in KP LUAD. Notably, single-cell clones derived from a KP;*Lgr5*$^{GFP\text{-}CreER/+}$ mouse LUAD formed heterogenous tumours comprised of Lgr5$^+$, porcupine$^+$ and Lgr5$^-$/porcupine$^-$ subpopulations (Extended Data Fig. 7a, b), indicating that considerable plasticity and heterogeneity in cellular states exist in the KP lung tumours[11]. On the basis of our lineage-tracing data, this heterogeneity is in part driven by cooperation between the porcupine$^+$ and Lgr5$^+$ subpopulations.

A subpopulation of Wnt-pathway-positive cells that have stem-like properties has recently been described in pancreatic ductal

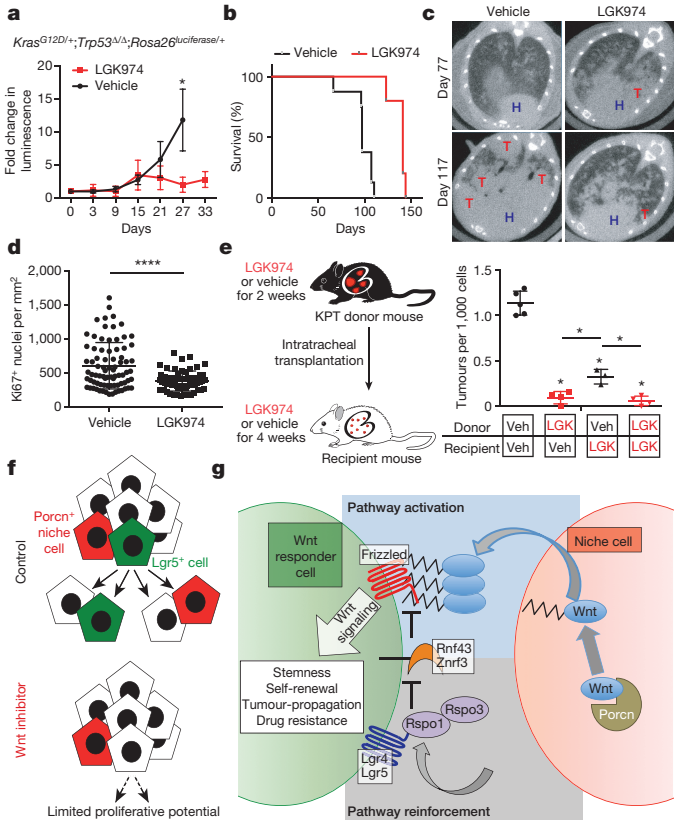

Figure 4 | Porcupine inhibition improves survival by suppressing proliferative potential in mice with lung adenocarcinoma. a, Fold change in bioluminescence signal in autochthonous KP LUAD tumours with a *Rosa26*$^{luciferase/+}$ allele in mice treated with LGK974 or vehicle. $n = 3$. **b**, Survival of mice with autochthonous KP LUAD tumours treated with LGK974 or vehicle starting at 77 days following tumour initiation. $P = 0.0008$; $n = 5$ (LGK974), 8 (vehicle). **c**, Lung μCT (microcomputed tomography) images of mice treated with vehicle or LGK974 at 77 days after tumour initiation and after 40 days on therapy (day 117). H, heart; T, tumour. **d**, Quantification of proliferating (Ki67$^+$) cells in autochthonous KP LUAD tumours two weeks after treatment with LGK974 or vehicle. $n = 80$ vehicle tumours, $n = 59$ LGK974 tumours. **e**, Quantification of the number of tdTomato$^+$ surface tumours in recipient mice. Data are mean ± s.d.; $^*P < 0.05$; $^{****}P < 0.0001$; Student's two-sided *t*-test (**a**, **b**, **d**); or two-way ANOVA (**e**). **f**, The outcome of Wnt inhibition in LUAD. Porcupine$^+$ niche cells provide Wnt to Lgr5$^+$ cells with robust proliferative potential, which can be suppressed by Wnt inhibitors. **g**, The niche for Wnt responder cells in LUAD. Lgr5$^+$ cells (green) reside next to porcupine$^+$ cells (red). Wnt5a, Wnt7a and Wnt7b, provided by porcupine$^+$ niche cells (red), bind frizzled on Wnt responder cells. Rspo1 and Rspo3, which bind Lgr4 and Lgr5, reinforce Wnt signalling by inhibiting Rnf43 and Znrf3 ubiquitin ligases that degrade frizzled[6]. Wnt is palmitoylated (serrated line) by porcupine, which is essential for Wnt secretion and binding to frizzled[3].

adenocarcinoma (PDAC) cell lines[12]. In line with these findings, we detected porcupine$^+$ cells in close proximity to a subpopulation of Lgr5$^+$ cells, which had increased proliferative potential in a PDAC GEMM (Extended Data Fig. 7c–f). Furthermore, Lgr5$^+$ stem-like cells have been described in intestinal adenomas[7]. We detected porcupine$^+$ cells in close proximity to the Lgr5$^+$ cells in *Apc*$^{\Delta/\Delta}$; *Lgr5*$^{GFP\text{-}CreER/+}$ mouse intestinal adenomas and porcupine expression in human colorectal carcinomas (Extended Data Fig. 7g, h). These results suggest that paracrine Wnt signals may maintain subpopulations of cancer cells in a stem-like state in other epithelial cancers.

To explore the relevance of increased Wnt signalling in human non-small cell lung cancer, we examined gene expression patterns in The Cancer Genome Atlas (TCGA) LUAD dataset. A ligand-stimulated Wnt gene expression signature[22] correlated with poor survival and higher tumour grade, and was independently prognostic in human LUAD, but not in squamous cell lung cancer (Extended Data Fig. 8a–c and Supplementary Table 1). We then extended this analysis to 34 additional human cancers within the TCGA dataset, and found similar correlations in PDAC and in mesothelioma (Extended Data Fig. 8d, e).

Given that KP LUAD cells respond to R-spondins through Lgr4 and Lgr5, we investigated the requirement for these genes in the KP model. CRISPR–Cas9-based combined inactivation of *Lgr4* and *Lgr5* in the KP model led to reduced lung tumour burden and prevented progression of adenomas to adenocarcinomas (Fig. 3d), similar to what was observed when targeting *Porcn* (Fig. 2g). Tumours that progressed into adenocarcinomas predominantly contained wild-type alleles or small non-frameshift mutations in *Lgr4* and *Lgr5* (Extended Data Fig. 8f–h). These data are consistent with a key role for Lgr4 and Lgr5 in the progression into adenocarcinomas. We detected expression of the Lgr4/Lgr5 ligands *Rspo1* and *Rspo3* in KP LUAD; these ligands localized predominantly to endothelial cells in the tumours (Extended Data Fig. 9a, b). Analogously, endothelial cells expressing R-spondin form a part of the niche for liver stem cells[23].

To identify the Wnt ligands and their frizzled (Fzd) receptors involved in LUAD, we performed qPCR on 84 Wnt-pathway-related genes in sorted KPT lung adenocarcinoma cells and their stroma. This analysis revealed very little expression of *Porcn* or Wnt ligands in the stroma, consistent with the cancer cells being the predominant source of Wnt ligands in LUAD (Extended Data Fig. 9c, d and Supplementary Table 2). Out of the 19 *Wnt* genes, *Wnt7a*, *Wnt5a* and *Wnt7b* were robustly expressed in LUAD (Extended Data Fig. 9c–e). *In situ* hybridization (ISH) showed that expression of these three Wnt ligands in KP LUAD was found in regions with Wnt pathway activation (Fig. 3e). Increased levels of *WNT5A*, *WNT3*, *WNT5B* and *WNT10A* in subpopulations of patients and, in particular, *WNT7B* were observed in human LUAD when compared to normal lung in the TCGA dataset (Extended Data Fig. 9f and Supplementary Table 3). We detected robust expression of 8 out of the 10 *Fzd* receptors and their *Lrp5* and *Lrp6* co-receptors in sorted KP LUAD cells (Extended Data Fig. 9g). Expression of *Fzd1*, *Fzd4* and *Fzd6* was increased in KP lung adenocarcinomas when compared to adenomas (Extended Data Fig. 9h). Of note, each of these receptors can be engaged by at least one of the three Wnt ligands identified in the current study[24].

We next explored inhibition of ligand-dependent Wnt signalling as a potential therapeutic strategy in LUAD. Treatment with LGK974 suppressed Wnt target genes, inhibited tumour growth, proliferation and prolonged survival of mice with advanced autochthonous KP LUAD tumours (Fig. 4a–d and Extended Data Fig. 10a, b). Furthermore, treatment of tumour donor mice with LGK974 markedly suppressed the tumour-forming ability of transplanted cells and reduced numbers of proliferative tumours in recipient mice (Fig. 4e and Extended Data Fig. 10c–e), suggesting that inhibiting Wnt can disrupt stem-like cells in LUAD (Fig. 4f).

Our results indicate that a subset of Kras and p53 mutant LUAD cells acts as a Wnt-producing niche for another cancer cell subpopulation that responds to the Wnt signal and has robust proliferative potential (Fig. 4g). Inhibiting porcupine disrupts Wnt secretion and activity in the niche, suppressing stem cell function in tumours, which ultimately translates into therapeutic benefit (Fig. 4f). Inhibitors of Wnt signalling or the R-spondin–Lgr5 axis have also shown efficacy in patient-derived xenograft models of LUAD[25,26]. We identified specific components of the Wnt–frizzled and R-spondin–Lgr5 signalling pathways that may serve as entry points for therapeutic approaches aimed at disrupting the interactions between niche cells and stem-like cells in LUAD (Fig. 4g).

In this study, we observed the emergence of porcupine$^+$ niche cells and Lgr5$^+$ stem-like cells as KP lung adenomas progress to adenocarcinomas. This transition is also associated with amplification of the mutant *Kras*^{G12D} locus and consequent increase in mitogen-activated protein kinase activity, as well as upregulation of tissue

repair pathways[27]. Therefore increased proliferation and activation of regenerative pathways may contribute to activation of Wnt signalling in adenocarcinoma. Notably, heterogeneous Wnt pathway activation and Lgr5$^+$ expression in progenitor-like cells is also observed during repair of normal epithelial tissues[8], suggesting that lung adenocarcinomas may be co-opting a latent tissue regenerative program upon progression. Our results indicate that Wnt pathway activity in a subset of cancer cells is essential for the maintenance of proliferative potential in LUAD, which presents a therapeutic opportunity for the treatment of lung adenocarcinoma and other epithelial cancers.

Online Content Methods, along with any additional Extended Data display items and Source Data, are available in the online version of the paper; references unique to these sections appear only in the online paper.

Received 6 July 2016; accepted 4 April 2017.
Published online 10 May 2017.

1. Greaves, M. & Maley, C. C. Clonal evolution in cancer. *Nature* **481,** 306–313 (2012).
2. Kreso, A. & Dick, J. E. Evolution of the cancer stem cell model. *Cell Stem Cell* **14,** 275–291 (2014).
3. Clevers, H., Loh, K. M. & Nusse, R. An integral program for tissue renewal and regeneration: Wnt signaling and stem cell control. *Science* **346,** 1248012 (2014).
4. Hogan, B. L. *et al.* Repair and regeneration of the respiratory system: complexity, plasticity, and mechanisms of lung stem cell function. *Cell Stem Cell* **15,** 123–138 (2014).
5. Herriges, M. & Morrisey, E. E. Lung development: orchestrating the generation and regeneration of a complex organ. *Development* **141,** 502–513 (2014).
6. de Lau, W., Peng, W. C., Gros, P. & Clevers, H. The R-spondin/Lgr5/Rnf43 module: regulator of Wnt signal strength. *Genes Dev.* **28,** 305–316 (2014).
7. Schepers, A. G. *et al.* Lineage tracing reveals Lgr5$^+$ stem cell activity in mouse intestinal adenomas. *Science* **337,** 730–735 (2012).
8. Huch, M. *et al.* Unlimited *in vitro* expansion of adult bi-potent pancreas progenitors through the Lgr5/R-spondin axis. *EMBO J.* **32,** 2708–2721 (2013).
9. Boumahdi, S. *et al.* SOX2 controls tumour initiation and cancer stem-cell functions in squamous-cell carcinoma. *Nature* **511,** 246–250 (2014).
10. Driessens, G., Beck, B., Caauwe, A., Simons, B. D. & Blanpain, C. Defining the mode of tumour growth by clonal analysis. *Nature* **488,** 527–530 (2012).
11. Meacham, C. E. & Morrison, S. J. Tumour heterogeneity and cancer cell plasticity. *Nature* **501,** 328–337 (2013).
12. Ilmer, M. *et al.* RSPO2 enhances canonical Wnt signaling to confer stemness-associated traits to susceptible pancreatic cancer cells. *Cancer Res.* **75,** 1883–1896 (2015).
13. Zheng, Y. *et al.* A rare population of CD24$^+$ITGB4$^+$Notch^{hi} cells drives tumor propagation in NSCLC and requires Notch3 for self-renewal. *Cancer Cell* **24,** 59–74 (2013).
14. Plaks, V., Kong, N. & Werb, Z. The cancer stem cell niche: how essential is the niche in regulating stemness of tumor cells? *Cell Stem Cell* **16,** 225–238 (2015).
15. Johnson, D. H., Schiller, J. H. & Bunn, P. A. Jr. Recent clinical advances in lung cancer management. *J. Clin. Oncol.* **32,** 973–982 (2014).
16. Juan, J., Muraguchi, T., Iezza, G., Sears, R. C. & McMahon, M. Diminished WNT → β-catenin → c-MYC signaling is a barrier for malignant progression of BRAF^{V600E}-induced lung tumors. *Genes Dev.* **28,** 561–575 (2014).
17. Pacheco-Pinedo, E. C. *et al.* Wnt/β-catenin signaling accelerates mouse lung tumorigenesis by imposing an embryonic distal progenitor phenotype on lung epithelium. *J. Clin. Invest.* **121,** 1935–1945 (2011).
18. Stewart, D. J. Wnt signaling pathway in non-small cell lung cancer. *J. Natl Cancer Inst.* **106,** djt356 (2014).
19. Nguyen, D. X. *et al.* WNT/TCF signaling through LEF1 and HOXB9 mediates lung adenocarcinoma metastasis. *Cell* **138,** 51–62 (2009).
20. Liu, J. *et al.* Targeting Wnt-driven cancer through the inhibition of porcupine by LGK974. *Proc. Natl Acad. Sci. USA* **110,** 20224–20229 (2013).
21. Konermann, S. *et al.* Genome-scale transcriptional activation by an engineered CRISPR–Cas9 complex. *Nature* **517,** 583–588 (2015).
22. Willert, J., Epping, M., Pollack, J. R., Brown, P. O. & Nusse, R. A transcriptional response to Wnt protein in human embryonic carcinoma cells. *BMC Dev. Biol.* **2,** 8 (2002).
23. Rocha, A. S. *et al.* The angiocrine factor Rspondin3 is a key determinant of liver zonation. *Cell Reports* **13,** 1757–1764 (2015).
24. Yu, H., Ye, X., Guo, N. & Nathans, J. Frizzled 2 and frizzled 7 function redundantly in convergent extension and closure of the ventricular septum and palate: evidence for a network of interacting genes. *Development* **139,** 4383–4394 (2012).
25. Gurney, A. *et al.* Wnt pathway inhibition via the targeting of frizzled receptors results in decreased growth and tumorigenicity of human tumors. *Proc. Natl Acad. Sci. USA* **109,** 11717–11722 (2012).
26. Chartier, C. *et al.* Therapeutic targeting of tumor-derived R-Spondin attenuates β-catenin signaling and tumorigenesis in multiple cancer types. *Cancer Res.* **76,** 713–723 (2016).
27. Feldser, D. M. *et al.* Stage-specific sensitivity to p53 restoration during lung cancer progression. *Nature* **468,** 572–575 (2010).

Supplementary Information is available in the online version of the paper.

Acknowledgements We thank D. McFadden and P. Sharp for critical reading of the manuscript and T. Papagiannakopoulos for helpful discussions; H. Clevers for *Lgr5$^{CreER/+}$* mice; Janssen Pharmaceuticals for human tissue; J. Roper for mouse colon adenoma tissue; R. T. Bronson for expertise in animal pathology; Y. Soto-Feliciano and S. Levine for massively parallel sequencing expertise; L. Gilbert, M. Horlbeck and J. Weissman for *Lgr5* CRISPR gene activation sgRNA sequences; A. Li for help with generation of TCGA data catalogues; M. Griffin, M. Jennings and G. Paradis for FACS support; E. Vasile for microscopy support; K. Cormier and the Hope Babette Tang (1983) Histology Facility for histology support; S. Bajpay, D. Canner, D. Garcia-Gali, R. Kohn, N. Marjanovich, K. Mercer, J. Replogle and R. Romero for help with experiments; K. Anderson, I. Baptista, A. Deconinck, J. Teixeira and K. Yee for administrative support; and the Swanson Biotechnology Center for excellent core facilities. This work was financially supported by the Transcend Program and Janssen Pharmaceuticals, the Lung Cancer Research Foundation, the Howard Hughes Medical Institute and, in part, by the Cancer Center Support (core) grant P30-CA14051 from the National Cancer Institute. T.T. is supported by the National Cancer Institute (K99 CA187317), the Sigrid Juselius Foundation, the Hope Funds for Cancer Research and the Maud Kuistila Foundation. T.J. is a Howard Hughes Medical Institute Investigator, a David H. Koch Professor of Biology and a Daniel K. Ludwig Scholar.

Author Contributions T.T. and T.J. designed and directed the study; T.T., K.W., Y.P. and R.A.W. performed all types of experiments reported in the study; F.J.S.-R. performed CRISPR gene activation experiments and analysed CRISPR-mutated loci; N.M.C. and K.H. performed gene expression analysis and N.M.C. performed ISH; N.S.J., L.S. and P.K. performed FACS; R.A. and N.R.K. performed molecular cloning and R.A. quantified Ki67$^+$ nuclei; X.G. performed cell culture experiments; M.C.-B. developed and used microcomputed tomography analysis methodology; W.X. generated shRNA reagents; A.B. conducted bioinformatic analyses; F.J.S.-R., N.S.J., Ö.H.Y., P.K. and A.B. provided conceptual advice; T.T. and T.J. wrote the manuscript with comments from all authors.

Author Information Reprints and permissions information is available at www.nature.com/reprints. The authors declare no competing financial interests. Readers are welcome to comment on the online version of the paper. Publisher's note: Springer Nature remains neutral with regard to jurisdictional claims in published maps and institutional affiliations. Correspondence and requests for materials should be addressed to T.J. (tjacks@mit.edu).

Reviewer Information *Nature* thanks H. Clevers and the other anonymous reviewer(s) for their contribution to the peer review of this work.

METHODS

Mice. Previously published *Kras*$^{LSL\text{-}G12D}$ (ref. 28), *Trp53*$^{flox/flox}$ (ref. 29), *Kras*$^{FSF\text{-}G12D}$ (ref. 30), *Trp53*$^{frt/frt}$ (ref. 31), *Rosa26*$^{LSL\text{-}tdTomato}$ (ref. 32), *Apc*$^{flox/flox}$ (ref. 33), *Rosa26*$^{LSL\text{-}luciferase}$ (ref. 34), *Rosa26*^{mTmG} (ref. 35), *Lgr5*$^{GFP\text{-}IRES\text{-}CreER/+}$ (ref. 36) and *Lgr5*$^{CreER/+}$ (ref. 8) gene-targeted mice were used in the study. All mice were maintained in a mixed Sv129/C57BL/6 genetic background. Tumours were induced in KP mice with 2.5×10^7 plaque-forming units (PFU) of AdCMV-Cre (Iowa), 2×10^8 PFU of AdSPC-Cre[23,37], 1×10^8 PFU of AdCMV-FlpO (Iowa) or 15–50,000 transforming units of lentiviral Cre, as previously described[38,39], in mice that were between 8–12 weeks of age. Approximately equal numbers of male and female mice were included in all experimental groups in all mouse experiments. Mice bearing lung tumours were treated with 10 mg per kg per day of LGK974 (ref. 20) resuspended in 0.5% carboxymethylcellulose (Sigma-Aldrich) and 0.5% Tween 80 (Sigma-Aldrich) or vehicle (0.5% carboxymethylcellulose and 0.5% Tween 80 only). Weights of mice were followed weekly. The growth of autochthonous *Kras*$^{G12D/+}$;*Trp53*$^{\Delta/\Delta}$;*Rosa26*$^{Luciferase/+}$ lung tumours was followed longitudinally by bioluminescence imaging, as previously described[34]. In brief, mice were anaesthetized by isoflurane inhalation, administered 100 mg kg^{-1} D-luciferin (Perkin Elmer) by intraperitoneal injection and imaged after 10 min, using the IVIS imaging system (Perkin Elmer). Such longitudinal imaging experiments were repeated three times and representative data from one such experiment is shown in Fig. 4a. Survival experiments were repeated three times and representative data from one such experiment is shown in Fig. 4b. For survival experiments, mice were randomized based on their tumour burden as assessed by μCT. Mice were assigned a tumour burden score ranging from 0 (no tumours) to 10 (lungs completely full of tumours), and experimental groups were formed such that each group had approximately equal average tumour burdens. Mice with tumour burden scores under 3 were excluded from the study. The health of the mice in all experiments was monitored daily by the investigators and/or veterinary staff at the Department of Comparative Medicine at Massachusetts Institute of Technology. Mice with a body condition score under 2 were humanely euthanized. Animal studies were approved by the Massachusetts Institute of Technology (MIT) Committee for Animal Care (institutional animal welfare assurance no. A-3125-01). The maximal tumour dimensions permitted by the MIT Committee for Animal Care were 2 cm across the largest tumour diameter and this limit was not reached in any of the experiments.

Isolation of primary mouse lung adenocarcinoma cells. Mice bearing *Kras*$^{G12D/+}$;*Trp53*$^{\Delta/\Delta}$;*Rosa26*$^{tdTomato/+}$ (KPT) or *Kras*$^{G12D/+}$;*Trp53*$^{\Delta/\Delta}$;*Rosa26*$^{tdTomato/+}$;*Lgr5*$^{GFP\text{-}CreER/+}$(KPT;*Lgr5*$^{GFP\text{-}CreER/+}$) LUAD tumours were euthanized 12–26 weeks after tumour induction and perfused with S-MEM (Gibco) through the right ventricle of the heart. Dissected lungs with tumours were dissociated in protease and DNase solution of the Lung Dissociation kit (Miltenyi Biotech) followed by mechanical dissociation using MACS C columns (Miltenyi Biotech) according to the manufacturer's instructions. The dissociated cells were filtered using a 100-μm strainer and red blood cells were lysed using ACK (Thermo Scientific), followed by staining with APC-conjugated CD31 (Biolegend, 102510), CD45 (BD, 559864), CD11b (eBioscience, 17-0112-82) and TER119 (BD, 557909) antibodies and dead cells with DAPI (Sigma-Aldrich). The same approach using the Tumour Dissociation kit (Miltenyi Biotech) was used to isolate *KPT*;*Lgr5*$^{GFP\text{-}CreER/+}$;*Pdx1*::*Cre* PDAC tumours cells when mice were 7 weeks of age.

Fluorescence-activated cell sorting (FACS) of stained primary cells was performed using a FACSAria sorter (BD) by gating for tdTomato$^+$/DAPI$^-$/APC$^-$ cells (total cancer cell fraction) for KPT tumours. For KPT;*Lgr5*$^{GFP\text{-}CreER/+}$ tumours, both tdTomato$^+$/DAPI$^-$/APC$^-$/GFP$^+$ (Lgr5$^+$ cancer cell fraction) and tdTomato$^+$/DAPI$^-$/APC$^-$/GFP$^-$ (Lgr5$^-$ cancer cell fraction) populations were sorted. Sorted cells were placed in 3D organotypic culture, transplanted intratracheally into NOD/SCID-γ (NSG) recipient mice, or subcutaneously into athymic *nu*/*nu* mice immediately after sorting (see below).

Transplantation of cancer cells into recipient mice. For intratracheal transplantation, 8–10-weeks-old immunodeficient NSG mice were anaesthetized, intubated as previously described[38], and allowed to inhale 15–50,000 sorted primary KP LUAD cancer cells resuspended in 30 μl of S-MEM (Gibco). For subcutaneous transplantation, 50–500,000 sorted primary KP LUAD cells, KP LUAD cell lines or single-cell clones derived from a *KP*;*Lgr5*$^{GFP\text{-}CreER/+}$ LUAD cell line were resuspended in 50% Matrigel/50% S-MEM and injected subcutaneously into both flanks of athymic *nu*/*nu* mice in a volume of 100 μl. Mice with transplant tumours were injected intraperitoneally with 1 mg of 5-ethynyl-2-deoxyuridine (EdU, Setareh Biotech) 4 h before euthanasia to label proliferating cells. EdU was detected in cryosections using the Click-iT EdU Alexa Fluor 488 Imaging kit (Thermo Scientific) according to the manufacturer's protocol. Lgr5$^+$ cells in close proximity to porcupine were detected by GFP and porcupine immunofluorescence. All GFP$^+$ cells were analysed as being immediately adjacent to at least one porcupine$^+$ cell, as double-positive for both GFP and porcupine, or as neither of the above (Fig. 3a). All transplantation experiments were reproduced three times.

Low-density 3D organotypic cell culture. 150–1,000 primary mouse KP LUAD cells, cells from established KP LUAD cell lines, or primary mouse PDAC cells were mixed in 50% Matrigel (BD) and 50% advanced DMEM/F12 (Gibco) and plated on 10 μl of Matrigel. The gel was allowed to solidify at 37 C, followed by addition of advanced DMEM/F12 (Thermo Scientific) supplemented with gentamicin (Thermo Scientific), penicillin–streptomycin (VWR), 10 mm HEPES (Thermo Scientific) and 2% heat-inactivated fetal bovine serum. For Wnt pathway manipulation, cultures were incubated with 1 μg ml^{-1} recombinant mouse (rm)R-spondin 1 (Sino Biological), 100 ng ml^{-1} rmWnt3a (R&D Sytstems), 500 ng ml^{-1} or 1 μg ml^{-1} rmDKK1 (R&D Systems) or 100 nM LGK974 (Medchem Express) for 6–14 days. Medium was changed every two days. At the end of the experiment, proliferating cells were labelled with 10 μM EdU for 4 h, followed by paraformaldehyde fixation and fluorescent labelling of proliferating cells using the Click-iT EdU Alexa Fluor 488 Imaging kit (Thermo Scientific), according to the manufacturer's protocol, in whole-mount preparations of tumour spheroids. Proliferating spheroids were quantified using a Nikon Eclipse 80i microscope: a spheroid was classified as a cluster of at least 10 cells, and a proliferating spheroid contained at least one EdU positive nucleus (proliferating cells were not observed in clusters of cells smaller than 10 cells). At least four replicate wells per condition were quantified in each experiment. Images were acquired using a Nikon A1R confocal microscope. Stimulation and inhibitor experiments were reproduced at least 10 times for each experimental condition.

Cell lines. Multiple cell lines were established from the mouse LUAD and PDAC KP GEMMs over the course of the study. The cell lines have not been authenticated. The cell lines were routinely tested for mycoplasma and found to be negative. At the time of conducting the experiments, no cell lines used were found to be listed in the ICLAC database of misidentified cell lines.

Immunohistochemistry. Tissues or tumour organoids were fixed in 10% formalin overnight and embedded in paraffin. Immunohistochemistry (IHC) was performed on a Thermo Autostainer 360 with or without haematoxylin counterstaining using antibodies against β-catenin (BD, 610153), Ki67 (Vector Labs, VP-RM04), glutamine synthetase (BD, 610517), or porcupine (Abcam, ab105543). Lungs from at least three tumour-bearing mice were analysed for each antibody. Livers and small intestines collected from three normal, healthy mice were used for β-catenin, glutamine synthetase and porcupine IHC. 65 human LUAD tumours samples in two separate tissue microarrays were analysed by IHC for β-catenin and porcupine. 5 human colorectal adenocarcinoma samples were stained with porcupine antibodies. All human tissue material was obtained commercially from Janssen Pharmaceuticals.

Tissue immunofluorescence. Mice were anaesthetized and perfused through the right cardiac ventricle with 1% paraformaldehyde. Lungs with tumours were dissected, immersed in 4% PFA overnight and frozen in OCT medium (Sakura Finetek). 7 μm sections were stained with antibodies to EpCAM (eBioscience, 17-5791-82), β-catenin (BD, 610153), GFP (Cell Signaling Technologies, 2956S; or Aves Labs, GFP-1020), CD11b (eBioscience, 17-0112-82) or porcupine (Abcam, ab105543). Lungs from at least three tumour-bearing mice were analysed for each antibody.

Quantification of cell proliferation in tumours. Digitally scanned images of Ki67-stained slides were created with the Aperio ScanScope AT2 at 20× magnification. Aperio's WebScope software was used to assess Ki67$^+$ density per tumour area. A built-in IHC nuclear image analysis algorithm was used to classify cells on the basis of the intensity of the nuclear Ki67 stain. Nuclei were classified from 0 to 3+; only nuclei with moderate nuclear staining (2+) or intense nuclear staining (3+) were considered Ki67$^+$. Tumour regions were outlined on WebScope before running the IHC nuclear image analysis algorithm such that the number of 2+ and 3+ cells was normalized to tumour area.

Quantitative PCR (qPCR). Total RNA was isolated from tumours or cells using the RNeasy plus kit (Qiagen) according to the manufacturer's instructions. cDNA was synthesized from 1 μg of RNA using the SuperScript VILO cDNA synthesis kit (Thermo Scientific). qPCR was performed in triplicates with 2 μl of diluted cDNA (1:10) using PerfeCTa SYBR Green FastMix (Thermo Scientific) on a Bio-Rad iCycler RT–PCR detection system. Expression was normalized to *Actb* or *Gapdh*. All oligonucleotides used in this study are listed in Supplementary Table 4. All qPCR experiments were reproduced using at least three biological replicates.

Alternatively, a Mouse WNT Signalling Pathway RT^2 Profiler PCR Array (Qiagen) was used according to the manufacturer's instructions. Raw expression values were thresholded to remove genes that were not detected or had low expression (maximum C_t value set to 33; 0 values set to 33). Array position to gene-name mapping details were retrieved from the manufacturer's website (www.pcrdataanalysis.sabiosciences.com). Expression values for all genes per array were normalized to the expression of the housekeeping gene *Gusb*. Three replicates of stroma samples and three replicates of tumour samples were compared to calculate $\log_2$ fold change and differential expression significance values (two-sided *t*-test).

Lentiviral shRNA-mediated gene silencing. shRNAs were cloned into lentiviral pLKO.1 vectors (Addgene, 10878) or into pTRIPZ (Dharmacon) vectors and

lentivirus was produced as previously described[40]. KP mouse LUAD cell lines were infected with the lentiviral vectors, followed by puromycin selection and, in the case of cells infected with the TRIPZ virus, incubation in 1 μg ml^{-1} doxycycline for four days and RNA extraction for testing target knockdown (Extended Data Fig. 2a and not shown). For combined *Lgr4* and *Lgr5* silencing experiments, cell lines expressing pLKO.1 driving *Lgr4* or *Lgr5* shRNAs were generated by puromycin selection, followed by infection with TRIPZ vectors driving miR30-based *Lgr4* or *Lgr5* shRNAs and turboRFP under the control of a TET-responsive promoter. Cells were incubated in 1 μg ml^{-1} doxycycline for two days and red fluorescent cells were sorted to generate pure cell lines expressing combinations of *Lgr4* and *Lgr5* shRNAs. All shRNA experiments were reproduced using at least three independent cell lines.

TOPFLASH assay. 10,000 of KP LUAD cells were plated in 100 μl of medium containing 10% FBS per well of a white-walled 96-well plate (Perkin Elmer). After 24 h, mouse KP LUAD cells were transfected using Attractene transfection reagent (Qiagen) according to the manufacturer's instructions with 150 ng of the TOPFLASH Firefly (M50) reporter[41] (Addgene, 12456) and 20 ng of pRL-SV40P *Renilla* (Addgene, 27163) constructs. In initial experiments, the Wnt-insensitive FOPFLASH (negative control) Firefly (M51) reporter[41] (Addgene, 12457) was used to rule out signal background (not shown). Cells were stimulated for 16 h with recombinant Rspo1 (1 μg ml^{-1}, Sino Biological), recombinant Wnt3a (100 ng ml^{-1}, R&D Systems) or their combination (RW) in advanced DMEM/F12 (Gibco), with supplements listed above. After stimulation, Firefly and *Renilla* signals were detected using Dual-Glo luciferase detection reagents (Promega) according to the manufacturer's instructions. A Tecan Infiniti 200 Pro plate reader and automated injector system was used to detect luminescence. To control for transfection efficiency, Firefly luciferase levels were normalized to *Renilla* luciferase levels to generate a measurement of relative luciferase units. Experimental data are presented as mean ± s.d. from three independent wells. All TOPFLASH experiments were reproduced using at least three independent cell lines.

Application of the synergistic activation mediator system to overexpress components of the R-spondin–Lgr5 axis. Catalytically dead Cas9 (dCas9)-based systems have recently emerged as powerful tools for transcriptionally activating endogenous genes[42]. Notably, these systems allow for overexpression of genes in their endogenous genomic context. To overexpress *Rspo2*, *Rspo3* or *Lgr5* in *Kras*$^{G12D/+}$;*Trp53*$^{\Delta/\Delta}$ LUAD cell lines, we used the SAM system, which is a three-component system based on: (1) the fusion of dCas9 to the transcriptional activator VP64 (a tandem repeat of four DALDDFDLDML sequences from *Herpes simplex* viral protein 16, VP16); (2) a modified gRNA scaffold containing two MS2 RNA aptamers; and (3) the MS2–p65–HSF1 tripartite synthetic transcriptional activator[21]. In this system, sgRNA-dependent recruitment of dCas9–VP64 and MS2–P65–HSF1 to the endogenous *Rspo2*, *Rspo3* or *Lgr5* loci results in potent transcriptional activation (Extended Data Fig. 1i–l).

Non-clonal *Kras*$^{G12D/+}$;*Trp53*$^{\Delta/\Delta}$;*Rosa26*$^{tdTomato/+}$ or *Kras*$^{G12D/+}$;*Trp53*$^{\Delta/\Delta}$;*Lgr5*$^{GFP\text{-}CreER/+}$ LUAD cells stably expressing dCas9–VP64–blast (Addgene, 61425) and MS2–P65–HSF1–hygro (Addgene, 61426) were generated using sequential lentiviral transduction and selection with blasticidin and hygromycin, respectively. To overexpress *Rspo2* or *Rspo3* we designed four independent sgRNA sequences targeting the *Rspo2* or *Rspo3* transcription start site; sgRNAs targeting the upstream region of the *Lgr5* gene were provided by L. Gilbert, M. Horlbeck and J. Weissman[43]. The sgRNAs were cloned into a lentiviral vector (Lenti-sgRNA-MS2-zeocin; Addgene, 61427) followed by transduction and zeocin selection of the aforementioned cell lines to generate *Kras*$^{G12D/+}$;*Trp53*$^{\Delta/\Delta}$;*Lgr5*$^{GFP\text{-}CreER/+}$ LUAD cell lines stably expressing all three components. These experiments were reproduced using three independent cell lines.

Cloning of lentiviral vectors. The 7TCF::luciferase-PGK::Cre, 7TCF::GFP-PGK-Cre and U6::sgRNA-EFS::Cre (pUSEC) lentivirus vectors were generated by Gibson assembly[44,45]. In brief, a 1.8-kb part corresponding to *7TCF::luciferase* or a 1.2-kb part corresponding to *7TCF::GFP* were amplified from 7TFP (Addgene, 24308, ref. 46) or 7TGP (Addgene, 24305, ref. 46) respectively, and fused with a 0.5-kb PGK promoter part, a 1.0-kb Cre cDNA part and the PmeI and BsrGI linearized LV1-5 (Addgene, 68411) part[44]. U6::sgRNA-EFS::Cre was generated by amplifying a 2.2-kb part corresponding to the U6-filler-chimeric gRNA backbone from pSECC (Addgene, 60820), and fused with a 0.25-kb EFS promoter part, a 1.0-kb Cre cDNA part and the PmeI and BsrGI linearized LV1-5 (Addgene, 68411) part[44]. Lentivirus was produced in 293FS* cells, as previously described[38]. Experiments using 7TCF::luciferase-PGK::Cre (Fig. 2a) were performed twice ($n = 15$ mice in total) and experiments using 7TCF::GFP-PGK-Cre (Fig. 2b) three times ($n = 19$ mice in total).

For generation of lentiviruses containing sgRNAs, three sgRNAs per gene targeting *Porcn*, *Lgr4* or *Lgr5* were designed using CRISPR Design[47], cloned into pSpCas9(BB)-2A-GFP (pX458, Addgene, 48138) as previously described[48], transfected into KP cells[49], and screened for efficiency by western blotting for porcupine protein or by massively parallel sequencing of the regions in *Lgr4* or *Lgr5* targeted by the respective sgRNAs (data not shown). The most efficient *Porcn* sgRNA was cloned into pSECC as previously described[49]. The most efficient *Lgr4* and *Lgr5* sgRNAs were cloned into the pUSEC vector together with a synthetic mouse/human U6 promoter (sU6), as previously described[50], to generate U6::sgLgr4-sU6::Lgr5-EFS::Cre (pU2SEC).

Measurement of Wnt signalling pathway activity in tumours *in vivo*. A KPT LUAD cell line was transduced with 7TCF::luciferase-PGK::Puro (7TFP) lentiviruses[46], selected for puromycin resistance, and transplanted subcutaneously into flanks of immunodeficient athymic *nu/nu* mice. Three weeks after transplantation, tumour burden was measured by registering tdTomato fluorescence using an IVIS imaging system (Perkin Elmer), followed by administration of 100 mg kg^{-1} D-Luciferin (Perkin Elmer) and detection of the luciferase signal (7TCF promoter activity). The luciferase signal was normalized to the tdTomato signal (Wnt pathway activity/total tumour burden). Quantification of Wnt pathway activity was performed every 24 h for a week in mice treated with 10 mg per kg per day of LGK974 or vehicle. The maximal tumour dimensions permitted by the MIT IACUC were 2 cm across the largest tumour diameter and this limit was not reached in these experiments. This experiment was performed twice.

Single-molecule mRNA *in situ* hybridization. Single-molecule *in situ* hybridization was performed on formalin-fixed paraffin-embedded tissues using the Advanced Cell Diagnostics RNAscope 2.5 HD Detection kit (322360). Catalogue numbers of the probes are 400331 (*Axin2*), 318321 (*Lgr4*), 312171 (*Lgr5*) and 404971 (*Porcn*), 401991 (*Rspo1*), 316791 (*Wnt5a*), 401121 (*Wnt7a*) and 401131 (*Wnt7b*). Lungs from three tumour-bearing mice were analysed.

Lineage-tracing of *Lgr5*$^{+}$ cells in KP tumours. We generated *Kras*$^{FSF\text{-}G12D/+}$;*Trp53*$^{frt/frt}$;*Lgr5*$^{CreER/+}$;*Rosa26*$^{mTmG/+}$ mice and induced lung tumours by intratracheal administration of AdCMV-FlpO. Lung tumours were collected, enzymatically dissociated and passaged *in vitro* for 8–10 passages to eradicate stromal cells from the cultures. Such early-passage cell lines were transplanted subcutaneously into flanks of NSG mice. When mice developed palpable tumours, they were administered a single tamoxifen pulse (20 mg kg^{-1}) or corn-oil vehicle control. Tumours were collected at 2 days or 14 days after tamoxifen administration and prepared for cryosectioning. Three sections 500 μm apart were prepared from each tumour and imaged under a fluorescence microscope. The number of GFP^{+} cells per section was quantified in nine tumours per time point.

μCT data acquisition and analysis. An eXplore CT 120 microcomputed tomography (μCT) system (Northridge Tri-Modality Imaging Inc.) was used for *in vivo* imaging. Mice were imaged under anaesthesia (induced at 3% isoflurane in oxygen, maintained at between 2–2.5% during imaging) in groups of 4 in a custom mouse holder. Scanner settings were as follows: 720 views, 360° rotation, 70 kVp, 50 mA, 32 ms integration time with 2 × 2 detector pixel binning (isotropic nominal resolution of 50 μm). Data were reconstructed using the Parallax Innovations GPU accelerated reconstruction engine for the eXplore CT120.

Tissue density values (in Hounsfield Units (HU)) for normal, air-filled lung parenchyma were determined by eye using MicroView software (Parallax Innovations). For the scanning conditions in this study a range of −550 to −300 HU was determined to represent the range of normal lung parenchyma values. A custom analysis script was created using MATLAB (MathWorks) to identify a region of interest (ROI) including the soft tissue of the mouse thorax. Within this region the volume of tissue within the 'healthy' density range was measured. Within this same volume minimum intensity projections (MinP) were created, both to confirm the accuracy of the ROI and to qualitatively assess lung pathology. For data visualization, the change in healthy lung volume was inverted to represent the change in tumour volume (Extended Data Fig. 10b). One experiment involving 9 mice treated with LGK974 and 11 mice treated with vehicle control was carried out to track changes in tumour volume (Extended Data Fig. 10b).

Human clinical data analyses. RNA-seq gene expression profiles of primary tumours and relevant clinical data of 488 patients with lung adenocarcinoma were obtained from The Cancer Genome Atlas (TCGA LUAD; http://cancergenome.nih.gov/). The previously published Wnt signalling geneset[22] (24 genes upregulated after stimulation with recombinant human WNT3A) was obtained from the Molecular Signatures Database (MSigDB)[51] and used to score individual patient expression profiles using ssGSEA[52,53]. Patients were stratified according to their correlation score, into top ($n = 115$) and bottom ($n = 114$) 20th percentile sets. Kaplan–Meier survival analysis was conducted between these sets of patients and the log-rank test was used to assess significance. Subsequently, the Kaplan–Meier survival analysis methodology was extended to assess significant survival differences across 35 TCGA cancer types using a similar strategy.

Additionally, the Cox proportional hazards regression model was used to analyse the prognostic value of the published geneset[22] across all patients within the TCGA LUAD cohort, in the context of additional clinical covariates. All univariate and multivariable analyses were conducted within a five-year survival timeframe. The following patient and tumour-stage clinical characteristics were used: signature (signature from ref. 22 strong versus weak correlation); gender

(male or female); age (years, continuous); smoking history (reformed >15 years versus non-smoker, reformed <15 years versus non-smoker, current smoker versus non-smoker); mutational load (derived as the number of non-silent mutations per 30 Mb of coding sequence, continuous); Union for International Cancer Control (UICC) TNM Stage specification (stage III/IV versus I/II); UICC *T* score specification (T2 versus T1, T3/T4 versus T1); UICC *N* score specification (N1/N2 versus N0). Hazard ratio proportionality assumptions for the Cox regression model were validated by testing for all interactions simultaneously ($P = 0.703$). Interaction between the signature of ref. 22 and TNM stage, *T* score and *N* score (significant covariates in the model) were tested using a likelihood ratio test to contrast a model consisting of both covariates with another model consisting of both covariates plus an interaction term. No statistically significant difference was found between the two models (TNM, $P = 0.8751$; *T* score, $P = 0.8204$; *N* score: $P = 0.8625$; likelihood ratio test). To test for statistically significant differences between the previously published[22] signature correlation scores across TCGA LUAD grade levels (*T* scores), the Kurskal–Wallis test was used to assess overall significance and the Mann–Whitney–Wilcoxon test was used to assess pairwise differences. All statistical analyses were conducted in R (http://www.R-project.org) and all survival analyses and were conducted using the survival package in R.

Finally, we analysed the expression of Wnt pathway genes present in the Mouse WNT Signalling Pathway RT^2. Profiler PCR Array (Qiagen) in the human TCGA LUAD data (Supplementary Table 3). Expression levels between 57 LUAD tumour samples and corresponding matched normal samples were analysed using empirical cumulative distribution function plots. Significance of different expression levels was assessed using the Kolmogorov–Smirnov test. For a more comprehensive analysis covering human orthologues of all WNT pathway genes tested on the mouse qPCR array, pairwise differential expression analysis (tumour versus normal, $n = 57$ each) was performed using EBSeq version 1.4.0 (ref. 54).

Massively parallel sequencing. CRISPR-Cas9-induced mutations were detected as before[59]. Briefly, genomic regions containing the sgPorcn, sgLgr4 or sgLgr5 target sequences were amplified using Herculase II Fusion DNA polymerase and gel purified (primer sequences are shown in Supplementary Table 4). Sequencing libraries were prepared from 50 ng of PCR product using the Nextera DNA Sample Preparation kit (Illumina) according to the manufacturer's instructions and sequenced on Illumina MiSeq sequencers to generate 150-bp, paired-end reads.

Bioinformatic analysis of target loci. CRISPR-Cas9-mutated loci were computationally analysed as before[59]. Briefly, illumina MiSeq reads (150 bp paired-end) were trimmed to 120 bp after reviewing base quality profiles, in order to remove lower quality 3′ ends. Traces of Nextera adapters were clipped using the FASTX toolkit (Hannon Laboratory, CSHL) and pairs with each read greater than 15 bp in length were retained. Additionally, read pairs where either read had 50% or more bases below a base quality threshold of Q30 (Sanger) were removed from subsequent analyses. The reference sequence of the target locus was supplemented with 10 bp genomic flanks and was indexed using an enhanced suffix array[55]. Read ends were anchored in the reference sequence using 10 bp terminal segments for a suffix array index lookup to search for exact matches. A sliding window of unit step size and a maximal soft-clip limit of 10 bp were used to search for possible anchors at either end of each read. For each read, optimal Smith–Waterman dynamic programming alignment[56] was performed between the reduced state space of the read sequence and the corresponding reference sequence spanning the maximally distanced anchor locations. Scoring parameters were selected to allow sensitive detection of short and long insertions and deletions while allowing for up to four mismatches and the highest scoring alignment was selected. Read pairs with both reads aligned in the proper orientation were processed to summarize the number of wild-type reads and the location and size of each insertion and deletion event. Overlapping reads within pairs were both required to support the event if they overlapped across the event location. Additionally, mutation events and wild-type reads were summarized within the extents of the sgRNA sequence and PAM site by considering read alignments that had a minimum of 20 bp overlap with this region. Mutation calls were translated to genomic coordinates and subsequently annotated using Annovar[57]. The alignment and post-processing code was implemented in C++ along with library functions from SeqAn[58] and SSW[59] and utility functions in Perl and R (http://www.R-project.org). Mutation calls were subjected to manual review using the Integrated Genomics Viewer (IGV)[60].

Statistics and reproducibility. Statistical analysis was carried out as indicated in the Figure legends, Extended Data Figure legends and in the Methods for each experiment. The data were found to meet the assumptions of the statistical tests. Variation was estimated for each group of data, the variance was found to be similar between the groups that were compared. No animals were excluded from any of the studies. The investigator was blinded with respect to group assignment for the quantification of 3D spheroids, proliferating (Ki67$^+$) cells and for the analysis of healthy lung volume by μCT. Power calculations were performed to estimate the sample size for experiments involving LGK974 treatment. In brief, to detect a difference of 30% in average survival between the two groups (effect size = 1.2 s.d. of survival based on Cohen's *d* (ref. 61) using untreated sample baseline survival from ref. 39) with 90% power, a minimum of five mice per group needed to be used.

Data availability. Massively parallel sequencing data are available in the NCBI/SRA data repository under accession number PRJNA379539. Source code and all other data are available from the authors upon reasonable request.

28. Jackson, E. L. *et al.* Analysis of lung tumor initiation and progression using conditional expression of oncogenic *K-ras*. *Genes Dev.* **15,** 3243–3248 (2001).
29. Marino, S., Vooijs, M., van der Gulden, H., Jonkers, J. & Berns, A. Induction of medulloblastomas in *p53*-null mutant mice by somatic inactivation of *Rb* in the external granular layer cells of the cerebellum. *Genes Dev.* **14,** 994–1004 (2000).
30. Young, N. P., Crowley, D. & Jacks, T. Uncoupling cancer mutations reveals critical timing of p53 loss in sarcomagenesis. *Cancer Res.* **71,** 4040–4047 (2011).
31. Lee, C. L. *et al.* Generation of primary tumors with Flp recombinase in *FRT*-flanked *p53* mice. *Dis. Model. Mech.* **5,** 397–402 (2012).
32. Madisen, L. *et al.* A robust and high-throughput Cre reporting and characterization system for the whole mouse brain. *Nat. Neurosci.* **13,** 133–140 (2010).
33. Kuraguchi, M. *et al.* Adenomatous polyposis coli (*APC*) is required for normal development of skin and thymus. *PLoS Genet.* **2,** e146 (2006).
34. Yeddula, N., Xia, Y., Ke, E., Beumer, J. & Verma, I. M. Screening for tumor suppressors: loss of ephrin receptor A2 cooperates with oncogenic *KRas* in promoting lung adenocarcinoma. *Proc. Natl Acad. Sci. USA* **112,** E6476–E6485 (2015).
35. Muzumdar, M. D., Tasic, B., Miyamichi, K., Li, L. & Luo, L. A global double-fluorescent Cre reporter mouse. *Genesis* **45,** 593–605 (2007).
36. Barker, N. *et al.* Identification of stem cells in small intestine and colon by marker gene *Lgr5*. *Nature* **449,** 1003–1007 (2007).
37. Sutherland, K. D. *et al.* Cell of origin of small cell lung cancer: inactivation of *Trp53* and *Rb1* in distinct cell types of adult mouse lung. *Cancer Cell* **19,** 754–764 (2011).
38. DuPage, M., Dooley, A. L. & Jacks, T. Conditional mouse lung cancer models using adenoviral or lentiviral delivery of Cre recombinase. *Nat. Protoc.* **4,** 1064–1072 (2009).
39. Jackson, E. L. *et al.* The differential effects of mutant *p53* alleles on advanced murine lung cancer. *Cancer Res.* **65,** 10280–10288 (2005).
40. Zuber, J. *et al.* Toolkit for evaluating genes required for proliferation and survival using tetracycline-regulated RNAi. *Nat. Biotechnol.* **29,** 79–83 (2011).
41. Korinek, V. *et al.* Constitutive transcriptional activation by a β-catenin-Tcf complex in APC$^{-/-}$ colon carcinoma. *Science* **275,** 1784–1787 (1997).
42. Hsu, P. D., Lander, E. S. & Zhang, F. Development and applications of CRISPR–Cas9 for genome engineering. *Cell* **157,** 1262–1278 (2014).
43. Horlbeck, M. A. *et al.* Compact and highly active next-generation libraries for CRISPR-mediated gene repression and activation. *eLife* **5,** e19760 (2016).
44. Akama-Garren, E. H. *et al.* A modular assembly platform for rapid generation of DNA constructs. *Sci. Rep.* **6,** 16836 (2016).
45. Gibson, D. G. *et al.* Enzymatic assembly of DNA molecules up to several hundred kilobases. *Nat. Methods* **6,** 343–345 (2009).
46. Fuerer, C. & Nusse, R. Lentiviral vectors to probe and manipulate the Wnt signaling pathway. *PLoS One* **5,** e9370 (2010).
47. Hsu, P. D. *et al.* DNA targeting specificity of RNA-guided Cas9 nucleases. *Nat. Biotechnol.* **31,** 827–832 (2013).
48. Ran, F. A. *et al.* Genome engineering using the CRISPR–Cas9 system. *Nat. Protoc.* **8,** 2281–2308 (2013).
49. Sánchez-Rivera, F. J. *et al.* Rapid modelling of cooperating genetic events in cancer through somatic genome editing. *Nature* **516,** 428–431 (2014).
50. Vidigal, J. A. & Ventura, A. Rapid and efficient one-step generation of paired gRNA CRISPR–Cas9 libraries. *Nat. Commun.* **6,** 8083 (2015).
51. Liberzon, A. *et al.* The molecular signatures database (MSigDB) hallmark gene set collection. *Cell Syst.* **1,** 417–425 (2015).
52. Subramanian, A. *et al.* Gene set enrichment analysis: a knowledge-based approach for interpreting genome-wide expression profiles. *Proc. Natl Acad. Sci. USA* **102,** 15545–15550 (2005).
53. Mootha, V. K. *et al.* PGC-1α-responsive genes involved in oxidative phosphorylation are coordinately downregulated in human diabetes. *Nat. Genet.* **34,** 267–273 (2003).
54. Leng, N. *et al.* EBSeq: an empirical Bayes hierarchical model for inference in RNA-seq experiments. *Bioinformatics* **29,** 1035–1043 (2013).
55. Abouelhoda, M. I., Kurtz, S. & Ohlebusch, E. Replacing suffix trees with enhanced suffix arrays. *J. Discrete Algorithms* **2,** 53–86 (2004).
56. Smith, T. F. & Waterman, M. S. Identification of common molecular subsequences. *J. Mol. Biol.* **147,** 195–197 (1981).
57. Wang, K., Li, M. & Hakonarson, H. ANNOVAR: functional annotation of genetic variants from high-throughput sequencing data. *Nucleic Acids Res.* **38,** e164 (2010).
58. Döring, A., Weese, D., Rausch, T. & Reinert, K. SeqAn an efficient, generic C++ library for sequence analysis. *BMC Bioinformatics* **9,** 11 (2008).
59. Zhao, M., Lee, W. P., Garrison, E. P. & Marth, G. T. SSW library: an SIMD Smith–Waterman C/C++ library for use in genomic applications. *PLoS One* **8,** e82138 (2013).
60. Thorvaldsdóttir, H., Robinson, J. T. & Mesirov, J. P. Integrative genomics viewer (IGV): high-performance genomics data visualization and exploration. *Brief. Bioinform.* **14,** 178–192 (2013).
61. Cumming, G. *Understanding the New Statistics: Effect sizes, Confidence Intervals, and Meta-Analysis* (Routledge, 2012).
62. Wang, B., Zhao, L., Fish, M., Logan, C. Y. & Nusse, R. Self-renewing diploid Axin2$^+$ cells fuel homeostatic renewal of the liver. *Nature* **524,** 180–185 (2015).

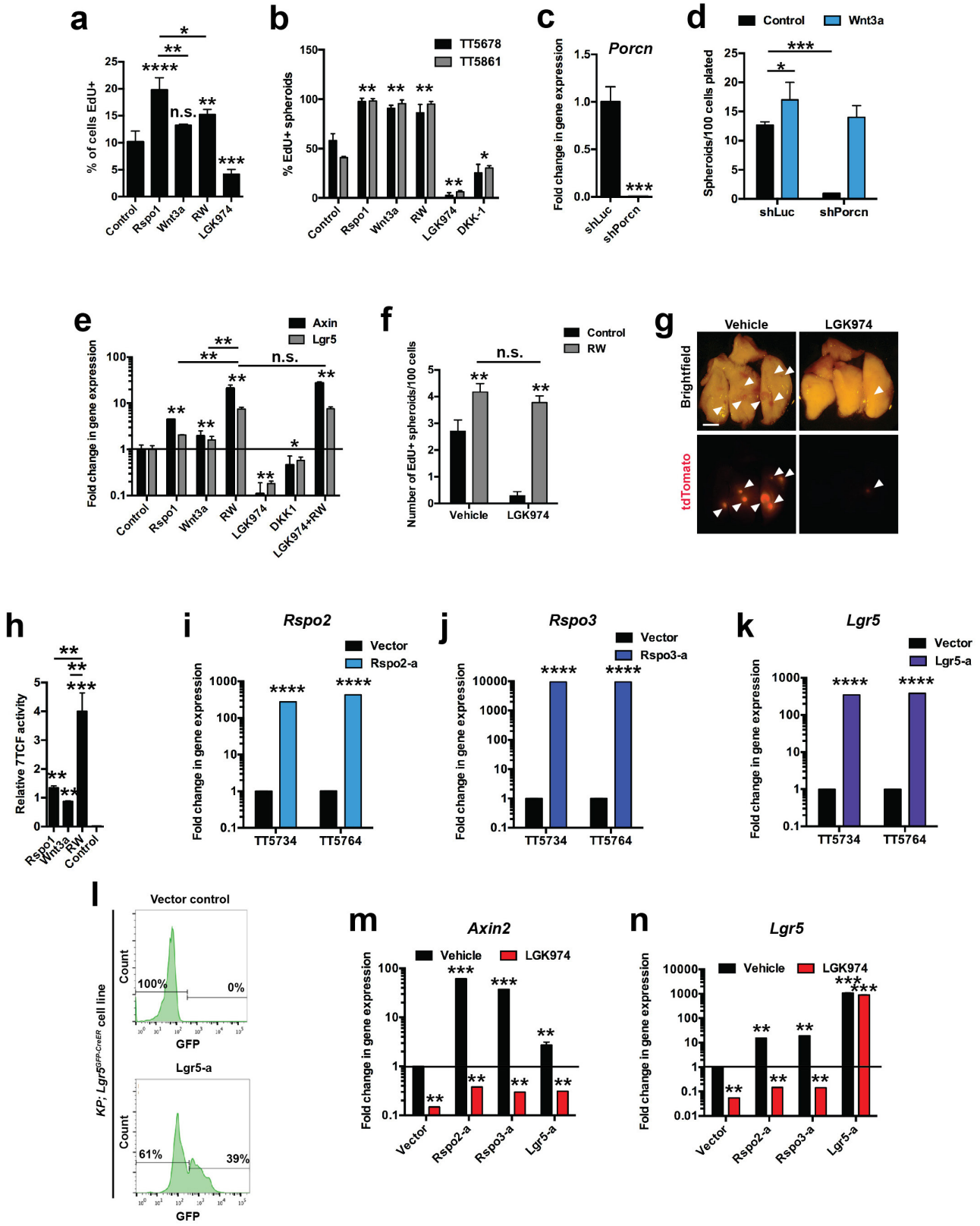

Extended Data Figure 1 | See next page for caption.

Extended Data Figure 1 | Inhibiting Wnt synthesis with the porcupine inhibitor LGK974 suppresses Wnt pathway activation by the R-spondin–Lgr5 axis in primary lung adenocarcinoma cultures. **a**, Percentage of EdU^+ (proliferating) cells in 3D cultures of KPT lung adenocarcinoma (LUAD) cells followed by Wnt pathway stimulation with Rspo1 (1 μg ml^{-1}), Wnt3a (100 ng ml^{-1}) or both (1 μg ml^{-1} Rspo1 and 100 ng ml^{-1} Wnt3a), or Wnt pathway inhibition with LGK974 (100 nM) or DKK1 (500 ng ml^{-1}) for seven days (starting at seven days after plating). EdU labelling was performed 16 h before analysis of proliferating cells by flow cytometry. $n = 6$ wells per condition. **b**, Percentage of spheroids proliferating in low-density 3D cultures of primary mouse KPT LUAD cells 14 days after plating. $n = 8$ wells per condition. Representative data from eight replicate experiments; TT5678 and TT5861 identify donor mice. **c**, qPCR of *Porcn* transcripts in sublines of a KP LUAD cell line expressing shRNAs targeting *Porcn* (shPorcn) or control shRNA (shLuc). Quantification of 3D tumour spheroids containing EdU^+ cells of KP LUAD cells expressing the indicated shRNAs in response to 100 ng ml^{-1} Wnt3a or control at six days after plating. Representative data of $n = 3$ technical replicates, the experiment was performed with three independent cell lines. **e**, Quantitative real-time PCR (qRT–PCR) analysis of *Axin2* and *Lgr5* transcripts in 3D cultures of primary KP LUAD cells following Wnt pathway stimulation with Rspo1 (1 μg ml^{-1}), Wnt3a (100 ng ml^{-1}) or both (1 μg ml^{-1} Rspo1 and 100 ng ml^{-1} Wnt3a), or Wnt pathway inhibition with LGK974 (100 nM) or DKK1 (1 μg ml^{-1}) for six days (starting at 10 days after plating). Representative data of $n = 3$ technical replicates. The experiment was carried out three times, each time with cells isolated from a different tumour-bearing mouse. **f**, Quantification of tumour spheroids containing EdU^+ cells per 100 primary KPT LUAD cells 14 days after plating. Combined treatment (1 μg ml^{-1} Rspo1 and 100 ng ml^{-1} Wnt3a); LGK974 (100 nM). $n = 8$ wells per condition. **g**, Recipient mouse lungs eight weeks after orthotopic transplantation of 30,000 primary $tdTomato^+$ (red) mouse KP LUAD cells. Arrowheads indicate $tdTomato^+$ tumours. Recipient mice were treated with 10 mg per kg per day LGK974 or vehicle for eight weeks, starting from the day of transplantation. Scale bar, 2 mm. The experiment was performed three times, each time with cells isolated from a different (donor) tumour-bearing mouse. **h**, Wnt-pathway activity measured by detection of firefly luciferase driven by a Wnt-sensitive 7TCF promoter (Topflash assay) in mouse KP LUAD cells stimulated for 24 h with the indicated growth factors. $n = 3$ technical replicates per condition. Representative data from experiments that were performed with four different cell lines. **i**–**k**, qPCR analysis of *Rspo2* (**i**), *Rspo3* (**j**) or *Lgr5* (**k**) transcripts in two independent mouse KP LUAD cell lines (TT5734 and TT5764) expressing SAM components[21] driving expression of the indicated genes. **l**, Flow cytometry analysis of GFP fluorescence in a KP LUAD cell line containing the $Lgr5^{GFP\text{-}CreER}$ reporter[36] expressing vector control (top) or an sgRNA targeting the transcription start site of *Lgr5* (bottom). **m**, **n**, qRT–PCR analysis of the Wnt target genes *Axin2* (**m**) and *Lgr5* (**n**) in 3D cultures of sublines of a KP LUAD cell line (TT5764) expressing the CRISPR-activator system driving expression of *Rspo2* (Rspo2-a), *Rspo3* (Rspo3-a) or *Lgr5* (Lgr5-a). Data are mean ± s.d.; $*P < 0.05$; $**P < 0.01$; $***P < 0.001$; $****P < 0.0001$; n.s., not significant; two-way ANOVA (**a**, **b**, **d**, **h**, **m**, **n**) or Student's two-sided *t*-test (**c**, **e**, **f**, **i**–**k**).

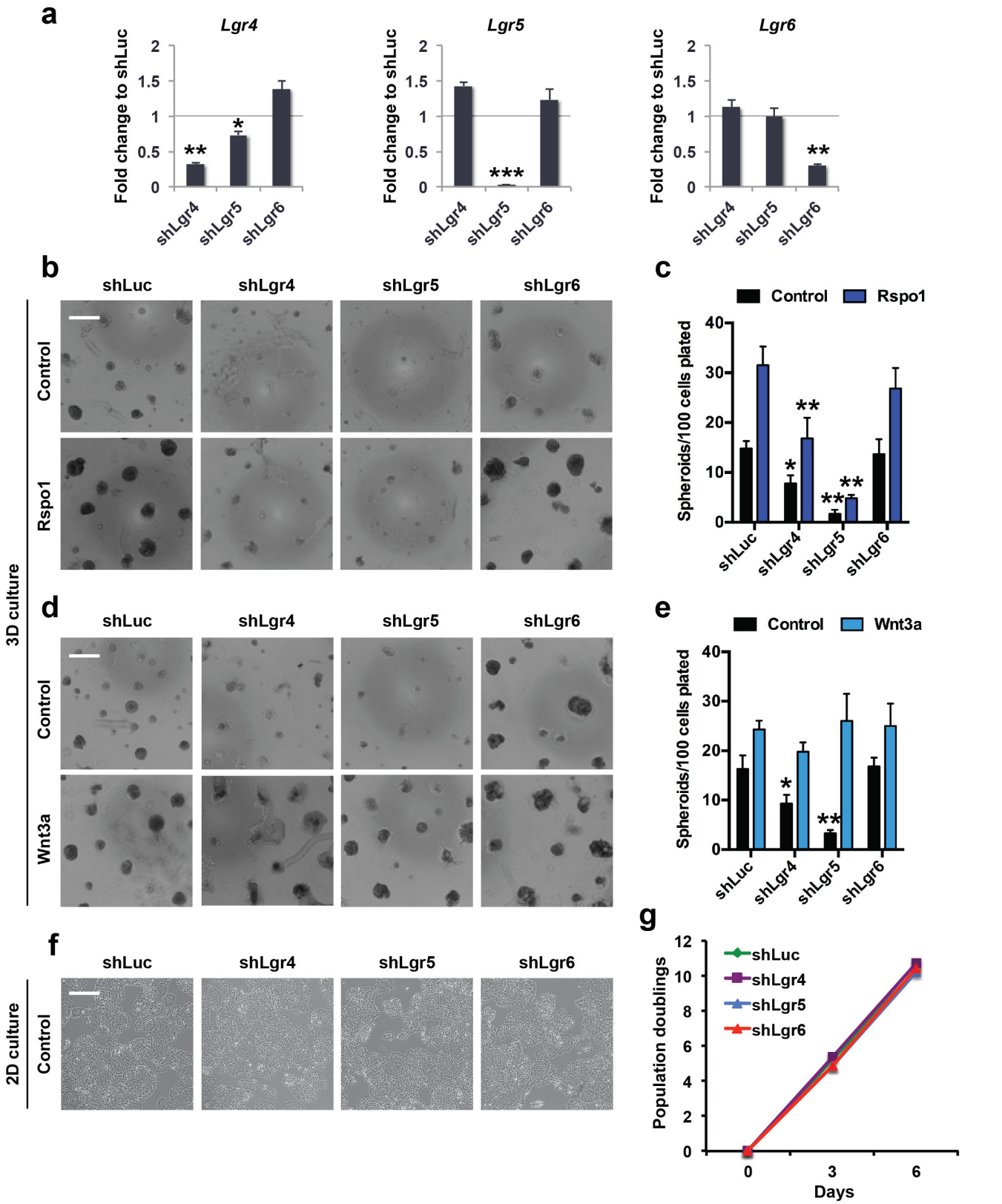

Extended Data Figure 2 | Lgr4 and Lgr5 are R-spondin receptors in lung adenocarcinoma. a, qRT–PCR analysis of *Lgr4*, *Lgr5* and *Lgr6* transcripts in sublines of a KP LUAD cell line stably expressing shLgr4, shLgr5, shLgr6 or shLuciferase (shLuc) control. Note minimal effects of the indicated shRNAs on other Lgr5 family members. $n = 3$ technical replicates per condition; representative data from three experiments carried out in different cell lines. **b**–**e**, Formation of 3D tumour spheroids of sublines of a KP LUAD cell line expressing the indicated shRNAs in response to 1 μg ml^{-1} Rspo1 (**b**, **c**) or 100 ng ml^{-1} Wnt3a (**d**, **e**) six days after plating. $n = 8$ wells per condition, representative data from three experiments carried out in different cell lines. **f**, **g**, No difference in cell morphology (**f**) or growth rate (**g**) in sublines of a KP LUAD cell line expressing shLgr4, shLgr5, shLgr6 or control shLuciferase (shLuc) over six days in two-dimensional cell culture. Scale bars, 500 μm (**b**, **d**) and 200 μm (**f**). Data are mean + s.d.; $^{*}P < 0.05$; $^{**}P < 0.01$; $^{***}P < 0.001$; Student's two-sided *t*-test (**a**) or two-way ANOVA (**c**, **e**, **g**). All experiments were performed three times, each time with a different KP LUAD cell line.

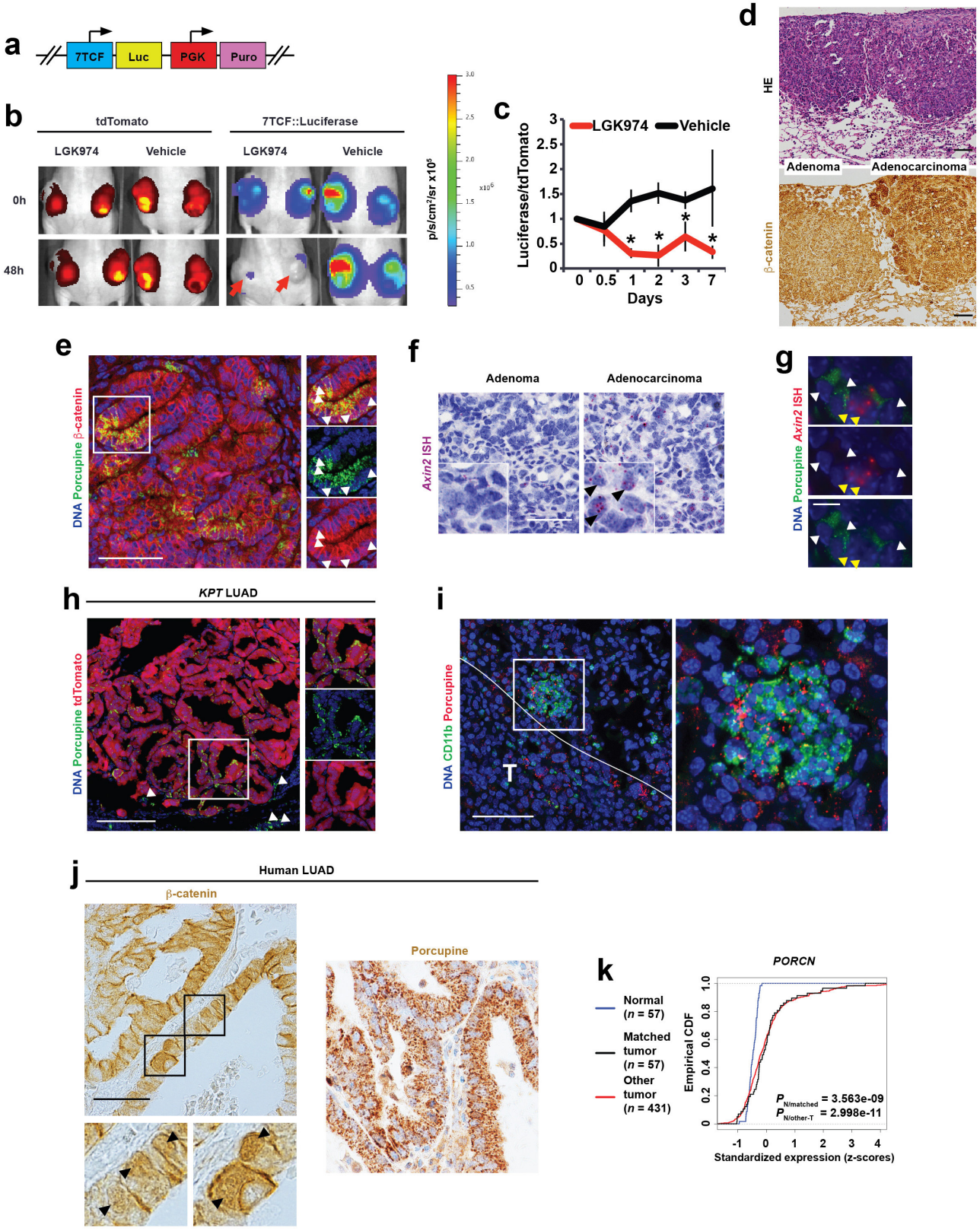

Extended Data Figure 3 | See next page for caption.

Extended Data Figure 3 | Wnt ligands predominantly produced by cancer cells drive activation of the Wnt signalling pathway in lung adenocarcinoma. a, Schematic representation of the lentiviral vector[46] used to transduce a KPT LUAD cell line, followed by puromycin selection. **b**, tdTomato and *7TCF::Luciferase* signals at baseline (0 h) and 48 h after treatment with 10 mg per kg per day LGK974 or vehicle. Red arrows indicate two subcutaneous tumours with reduced 7TCF-dependent bioluminescence in response to 48 h of LGK974 treatment. **c**, Suppression of 7TCF-driven bioluminescence by LGK974 relative to the tdTomato signal in mice with subcutaneous transplants of the KPT LUAD cell line stably expressing the 7TCF::Luciferase-PGK-Puro lentivirus. $n = 6$ tumours, three mice per group; representative data from two independent experiments. Data are mean ± s.d.; Student's two-sided *t*-test. **d**, Haematoxylin and eosin (HE) or β-catenin staining in KP adenomas or in adenocarcinomas. **e**, Immunofluorescence for β-catenin (red) and porcupine (green) in a KP LUAD. **f**, ISH for *Axin2* mRNA (purple, arrowheads) in KP lung adenomas or adenocarcinomas. **g**, Immunofluorescence for porcupine (green, white arrowheads) and ISH for *Axin2* (red, yellow arrowheads) in a KP LUAD. **h**, Immunofluorescence for porcupine (green) in an autochthonous grade 3 KPT adenocarcinoma. Arrowheads indicate peritumoural porcupine$^+$ cells, which are tdTomato$^-$ (that is, not cancer cells). **i**, CD11b (green) and porcupine (red) immunofluorescence in a peritumoural region. White line delineates the tumour (T). **j**, Immunohistochemistry for β-catenin or porcupine in human LUAD. Arrowheads indicate cells with nuclear β-catenin. 65 human LUAD tumours in two tissue microarrays were analysed. Scale bars, 100 μm (**d**, **e**, **h**–**j**), 50 μm (**f**) and 10 μm (**g**). **k**, Comparison of *PORCN* gene expression in tumours versus normal tissue in the TCGA lung adenocarcinoma cohort: Empirical cumulative density function (CDF) plots of standardized gene expression values are shown. A right-shift indicates relatively higher expression, with *P* values indicated to assess statistical significance (Kolmogorov–Smirnov test).

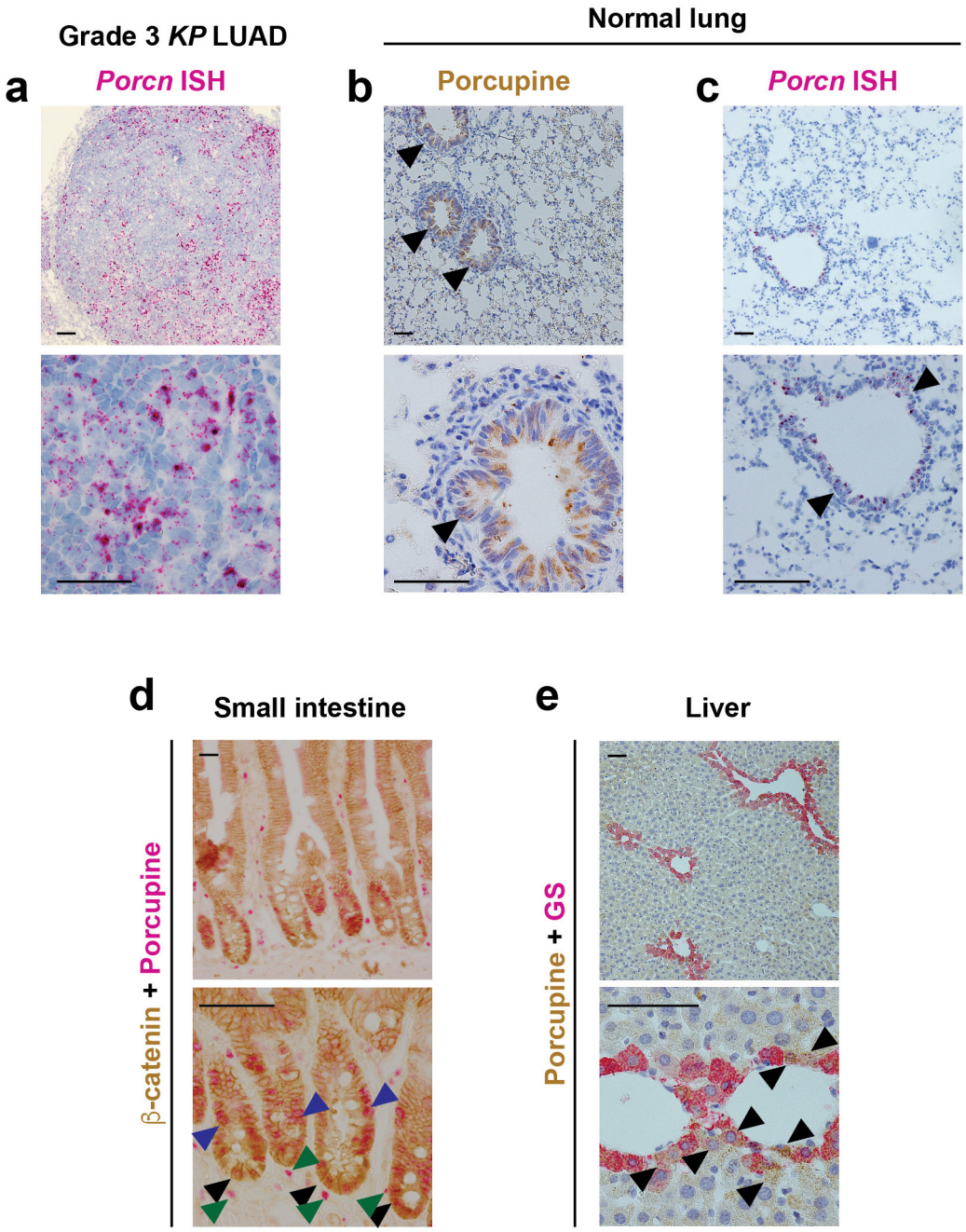

Extended Data Figure 4 | Expression of porcupine in lung adenocarcinoma, the normal lung and in stem cell niches of the intestine and liver. a, ISH for *Porcn* in a grade 3 KP lung adenocarcinoma. **b**, **c**, Immunohistochemistry for porcupine (brown) (**b**), or *Porcn* ISH in the normal lung (**c**). Arrowheads indicate porcupine expression in bronchioles. **d**, Immunohistochemistry for β-catenin (brown) and porcupine (purple) in the small intestine. Note porcupine expression in intestinal crypts (black arrowheads), the location of $Lgr5^+$ intestinal stem cells[36], as well as in transit-amplifying cells (blue arrowheads) and stromal cells (dark green). **e**, Immunostaining for porcupine (brown) and glutamine synthetase (GS, purple) expression localizes to areas around the central vein of the liver (**e**), coinciding with the location of $Lgr5^+Axin2^+$ liver stem cells[8,62]. Scale bars, 100 μm.

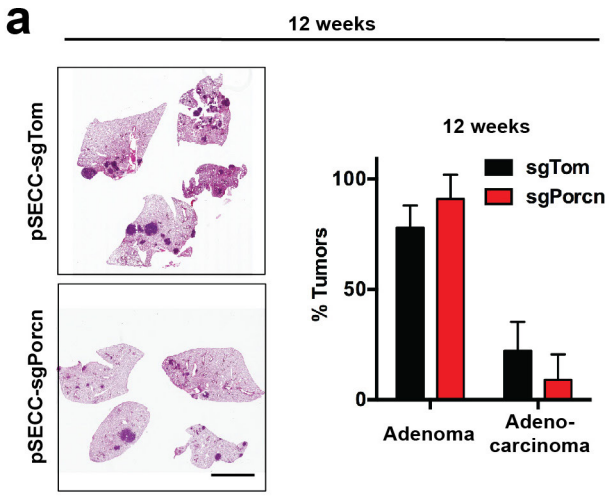

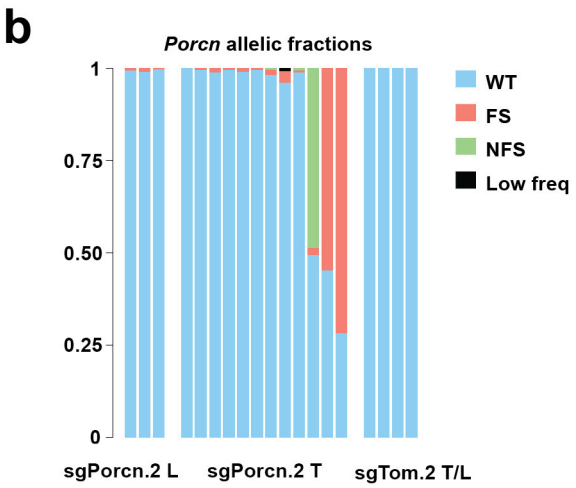

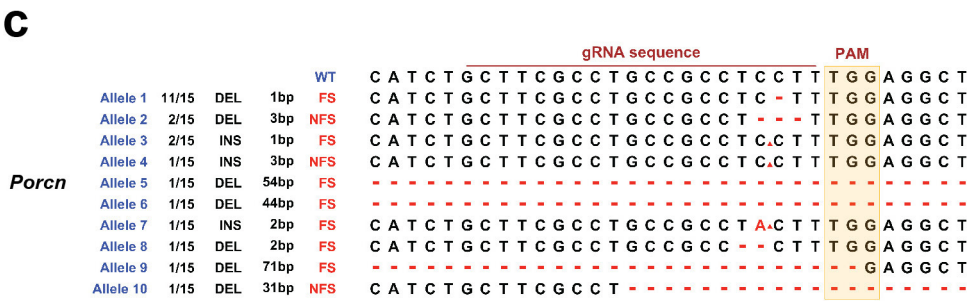

Extended Data Figure 5 | Analysis of the *Porcn* locus following CRISPR–Cas9-mediated genome editing *in vivo*. **a**, Haematoxylin and eosin staining of KP LUAD-bearing lungs generated with pSECC–sgTom or pSECC–sgPorcn and quantification of the proportion of adenomas versus adenocarcinomas at 12 weeks after tumour initiation. Scale bar, 2 mm. Data are mean ± s.d.; Student's two-sided *t*-test; $n = 5$ mice per group. **b**, Massively parallel sequencing analysis of allelic fractions of the *Porcn* locus in lung lobes containing microscopic tumours (sgPorcn.2 L) or microdissected macroscopic tumours (sgPorcn.2 T) induced in KP mice using pSECC–sgPorcn.2, or in lung lobes or macroscopic tumours induced in KP mice using pSECC–sgTom.2 (sgTom.2 T/L). FS, frameshift mutation; low freq, low-frequency mutation event; NFS, non-frameshift mutation; WT, wild-type read. Note predominantly wild-type or non-frameshift reads in microdissected tumours, whereas mutations in tumours containing microscopic tumours have introduced frameshifts. The large contribution of wild-type reads in sgPorcn.2 L samples is owing to domination of the normal stroma in whole-lobe samples, whereas wild-type reads in sgPorcn.2 T indicate cancer cells where genome editing did not function, as in whole-tumour samples, tumour cells are expected to contribute at least 50% (ref. 49). **c**, Qualitative analysis of mutations introduced by sgPorcn.2 *in vivo*. bp, base pair (indicates the size of the insertion or deletion); INS, insertion; DEL, deletion. Ratio indicates frequency of event across the 15 samples analysed.

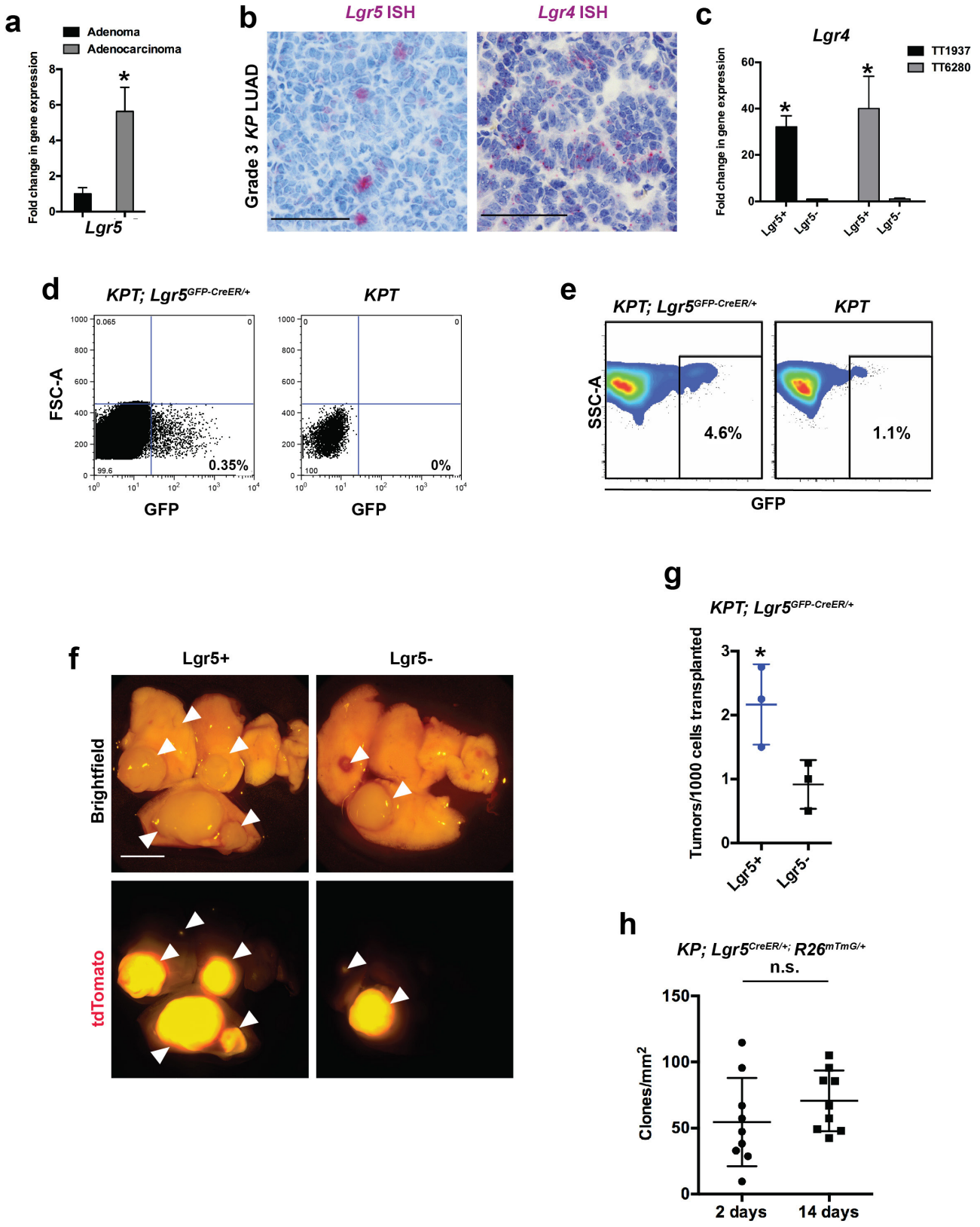

Extended Data Figure 6 | See next page for caption.

Extended Data Figure 6 | Lgr5 and Lgr4 are expressed in lung adenocarcinoma and Lgr5 marks cells with increased tumour-forming ability. a, qPCR analysis of *Lgr5* gene expression in KP LUAD tumours microdissected at 9 weeks (adenomas) or 20 weeks (adenocarcinomas) after initiation with adenoviral Cre. $n = 6$ tumours per group. **b**, ISH for *Lgr5* or *Lgr4* mRNA (purple) in grade 3 KP LUAD adenocarcinomas 12 weeks after tumour induction with AdCre. **c**, **d**, FACS sorting (**d**) of $Lgr5^{+}$ (GFP^{+}) cells in a cultured KP LUAD cell line containing the $Lgr5^{GFP\text{-}CreER/+}$ reporter allele (KP;$Lgr5^{GFP\text{-}CreER/+}$), followed by qRT–PCR analysis (**c**) of *Lgr4* expression in $Lgr5^{+}$ cells in two independent cell lines (TT1937 and TT6280). This experiment was performed once. **e**, FACS of GFP^{+} and GFP^{-} cells isolated from KPT;$Lgr5^{GFP\text{-}CreER/+}$ primary LUAD 14 weeks after tumour initiation with intratracheally administered AdCre. The FACS plot is gated on $tdTomato^{+}CD11b^{-}CD31^{-}CD45^{-}TER119^{-}$ cells. Note bleeding of the tdTomato signal to the GFP channel in the panel on the right. Gates were drawn as shown to increase cell yield at the cost of purity to enrich for $Lgr5^{+}$ cells. Such FACS sorting was performed on 21 KPT;$Lgr5^{GFP\text{-}CreER/+}$ mice. **f**, Recipient mouse lungs, 12 weeks after orthotopic transplantation of 15,000 primary $Lgr5^{+}tdTomato^{+}$ or $Lgr5^{-}tdTomato^{+}$ primary mouse LUAD cells. Arrowheads indicate $tdTomato^{+}$ tumours (red). Representative data from three replicate experiments. **g**, Quantification of tumours per 1,000 cells in recipient mouse lungs 12 weeks after orthotopic transplantation of 15,000 primary $Lgr5^{+}/tdTomato^{+}$ or $Lgr5^{-}/tdTomato^{+}$ primary mouse LUAD cells. $n = 3$ recipient mice per group; representative data from three replicate experiments. **h**, Number of membrane-associated GFP^{+} ($mGFP^{+}$) clones following lineage-tracing in established subcutaneous KP;$Lgr5^{CreER/+}$;$Rosa26^{LSL\text{-}mTmG/+}$ LUAD primary transplants (see Fig. 3c). $n = 9$ tumours/time point. Scale bars, 2 mm (**f**) and 100 μm (**b**). Data are mean ± s.d.; $^{*}P < 0.05$; n.s., not significant; Student's two-sided *t*-test (**a**, **c**, **g**, **h**).

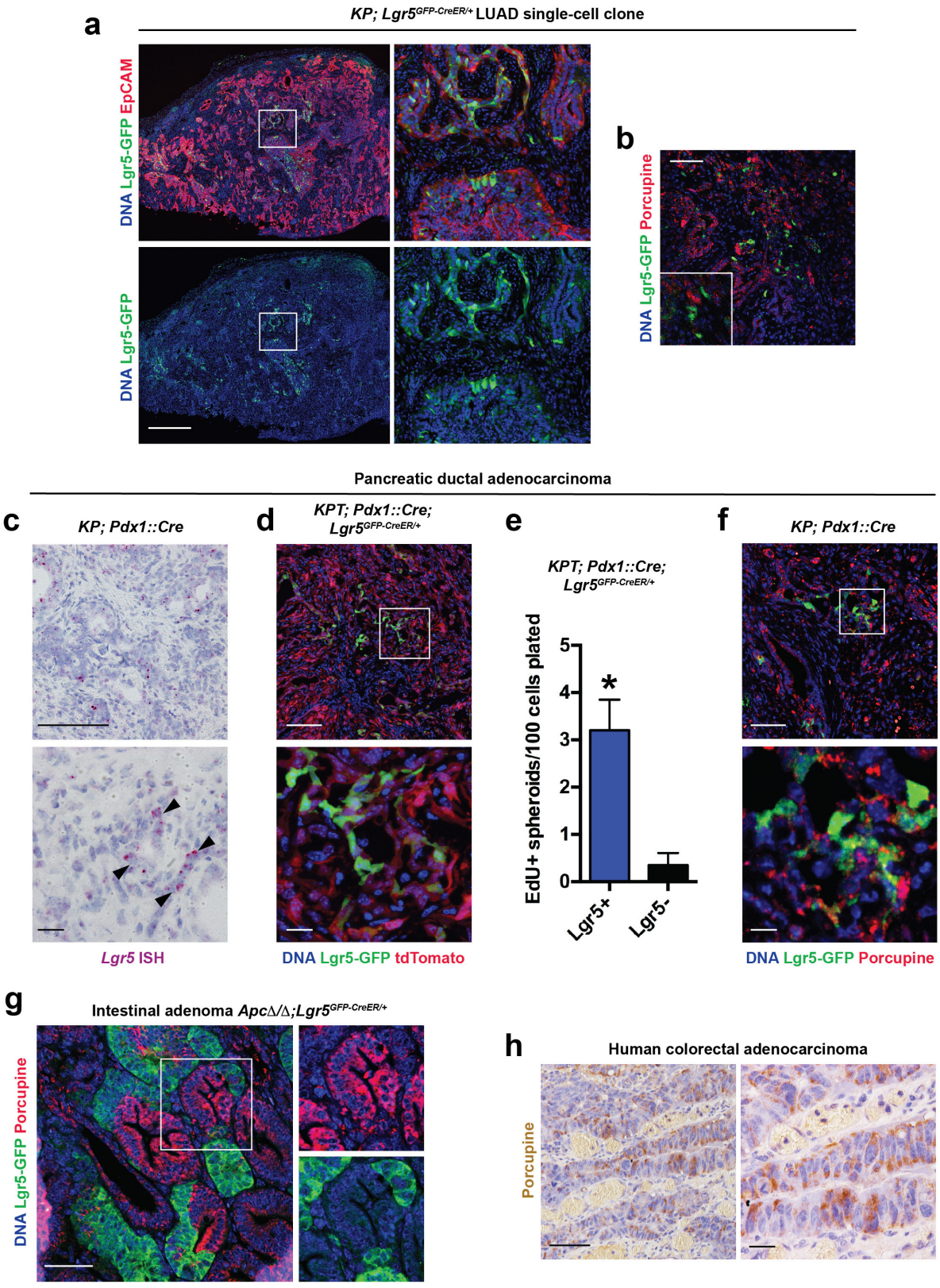

Extended Data Figure 7 | See next page for caption.

Extended Data Figure 7 | Phenotypic plasticity of Lgr5$^+$ cells that reside in porcupine$^+$ niches in lung, pancreatic and colon tumours. a, Immunofluorescence for GFP (green) and EpCAM (red) in a subcutaneous transplant established from a single-cell clone of a KPT;*Lgr5*$^{CreER/+}$ cell line. **b**, Immunofluorescence for GFP (green) and porcupine (red) in a subcutaneous transplant established from a single-cell clone of a KPT;*Lgr5*$^{CreER/+}$ cell line. **a**, **b**, Data are representative of four replicate experiments, each with a different KP;*Lgr5*$^{CreER/+}$ cell line. **c**, ISH for *Lgr5* mRNA (purple) in KP;*Pdx1*::*Cre* PDAC. Representative of three PDAC tumours analysed. **d**, Immunofluorescence staining for GFP (green) in a tdTomato$^+$ (red) autochthonous KP;*Lgr5*$^{GFP\text{-}CreER/+}$;*Rosa26*$^{tdTomato/+}$;*Pdx1*::*Cre* PDAC. **e**, Quantification of primary spheroids containing EdU$^+$ cells per 100 Lgr5$^+$tdTomato$^+$ or Lgr5$^-$tdTomato$^+$ primary mouse PDAC cells plated. $n = 4$ wells per group. Data are mean ± s.d.; $^*P < 0.05$; Student's two-sided *t*-test. **f**, Immunofluorescence staining for GFP (green) and porcupine (red) in autochthonous KP;*Lgr5*$^{GFP\text{-}CreER/+}$;*Pdx1*::*Cre* PDAC. Note juxtaposition of Lgr5$^+$ and porcupine$^+$ cells in the tumours. **d**, **f**, Representative data from six KP;*Lgr5*$^{GFP\text{-}CreER/+}$;*Pdx1*::*Cre* PDAC tumours analysed. **g**, Immunofluorescence staining for GFP (green) and porcupine in an autochthonous *Apc*$^{\Delta/\Delta}$;*Lgr5*$^{GFP\text{-}CreER/+}$intestinal adenoma. Again, note juxtaposition of Lgr5$^+$ and porcupine$^+$ cells in the tumours. $n = 3$ tumour samples. **h**, Immunohistochemistry for porcupine (brown) in human colorectal adenocarcinoma. Five human colorectal adenocarcinoma samples were analysed. Scale bars, 1 mm (**a**), 100 μm (**b**, **c**, **d**, **f** and **h** (top), **g**) and 10 μm (**c**, **d**, **f** and **h** (bottom)).

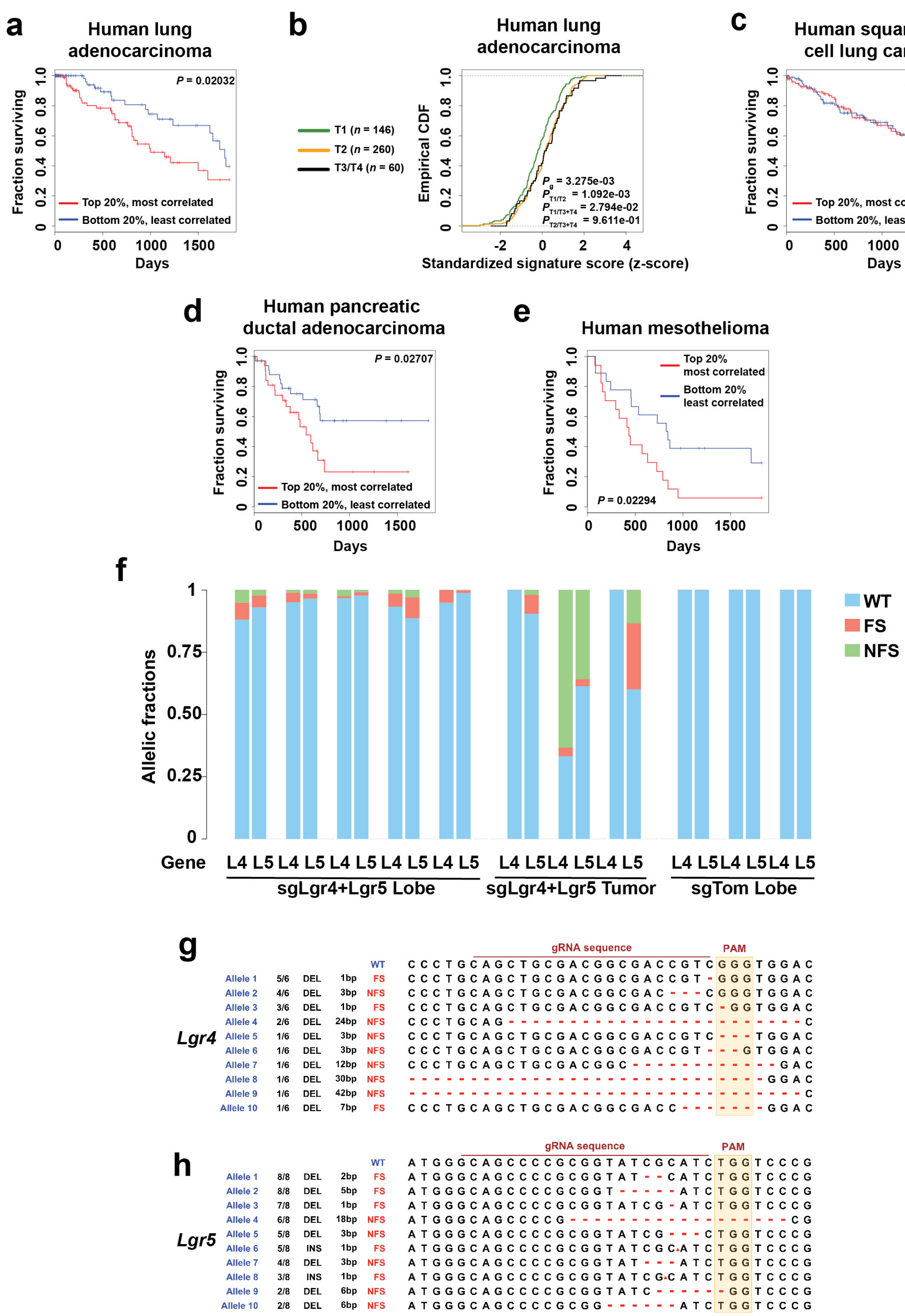

Extended Data Figure 8 | See next page for caption.

Extended Data Figure 8 | Wnt pathway activation correlates with poor survival in human lung adenocarcinoma, pancreatic ductal adenocarcinoma and mesothelioma, but not in human squamous cell lung cancer; analysis of the *Lgr4* and *Lgr5* loci following CRISPR–Cas9-mediated genome editing *in vivo*. **a**, Kaplan–Meier survival curve comparing the 20% strongest (red, $n = 91$) and weakest (blue, $n = 92$) correlations of the Wnt signature from ref. 22 and patient samples from the TCGA lung adenocarcinoma cohort. **b**, Empirical CDF plots of standardized gene expression values showing a correlation between the Wnt pathway activation gene expression signature correlation score and histological grade of primary tumours. A right-shift indicates relatively higher expression, with *P* values indicated to assess statistical significance (Kolmogorov–Smirnov test). **c**–**e**, Kaplan–Meier survival curves comparing the 20% strongest (red) and weakest (blue) correlations of the Wnt signature from ref. 22 and patients samples from the TCGA squamous cell lung cancer (**c**, most-correlated (red) $n = 100$, least-correlated (blue) $n = 100$), pancreatic ductal adenocarcinoma (**d**, most-correlated (red) $n = 34$, least-correlated (blue) $n = 34$) and mesothelioma (**e**, most-correlated (red) $n = 17$, least-correlated (blue) $n = 18$) cohorts. **f**, Massively parallel sequencing analysis of allelic fractions of the *Lgr4* and *Lgr5* loci in lung lobes containing microscopic tumours (lobe) or microdissected macroscopic tumours (tumour) induced in $Kras^{LSL\text{-}G12D/+}$;$Trp53^{flox/flox}$;$Rosa26^{LSL\text{-}Cas9+2a+eGFP/+}$ mice using *hU6*::*sgLgr4-sU6*::*sgLgr5-EFS*::*Cre* (pU2SEC) or *hU6*::*sgTom-EFS*::*Cre* (pUSEC) lentiviral vectors. FS, frameshift mutation; NFS, non-frameshift mutation; WT, wild-type read. Note predominantly wild-type or non-frameshift reads in microdissected tumours, whereas mutations in tumours containing microscopic tumours have introduced frameshifts. The large contribution of wild-type reads in lobe samples is owing to domination of the normal stroma in whole-lobe samples, whereas wild-type reads in *Lgr4*/*Lgr5* co-targeted tumours indicate cancer cells where genome editing did not function, as in whole tumour samples, tumour cells are expected to contribute at least 50% (ref. 49). **g**, **h**, Qualitative analysis of mutations introduced by sgLgr4 or sgLgr5 *in vivo*. bp, base pair (indicates size of insertion/deletion); INS, insertion; DEL, deletion. Ratio indicates frequency of event across all samples analysed. *P* values are indicated (log-rank test).

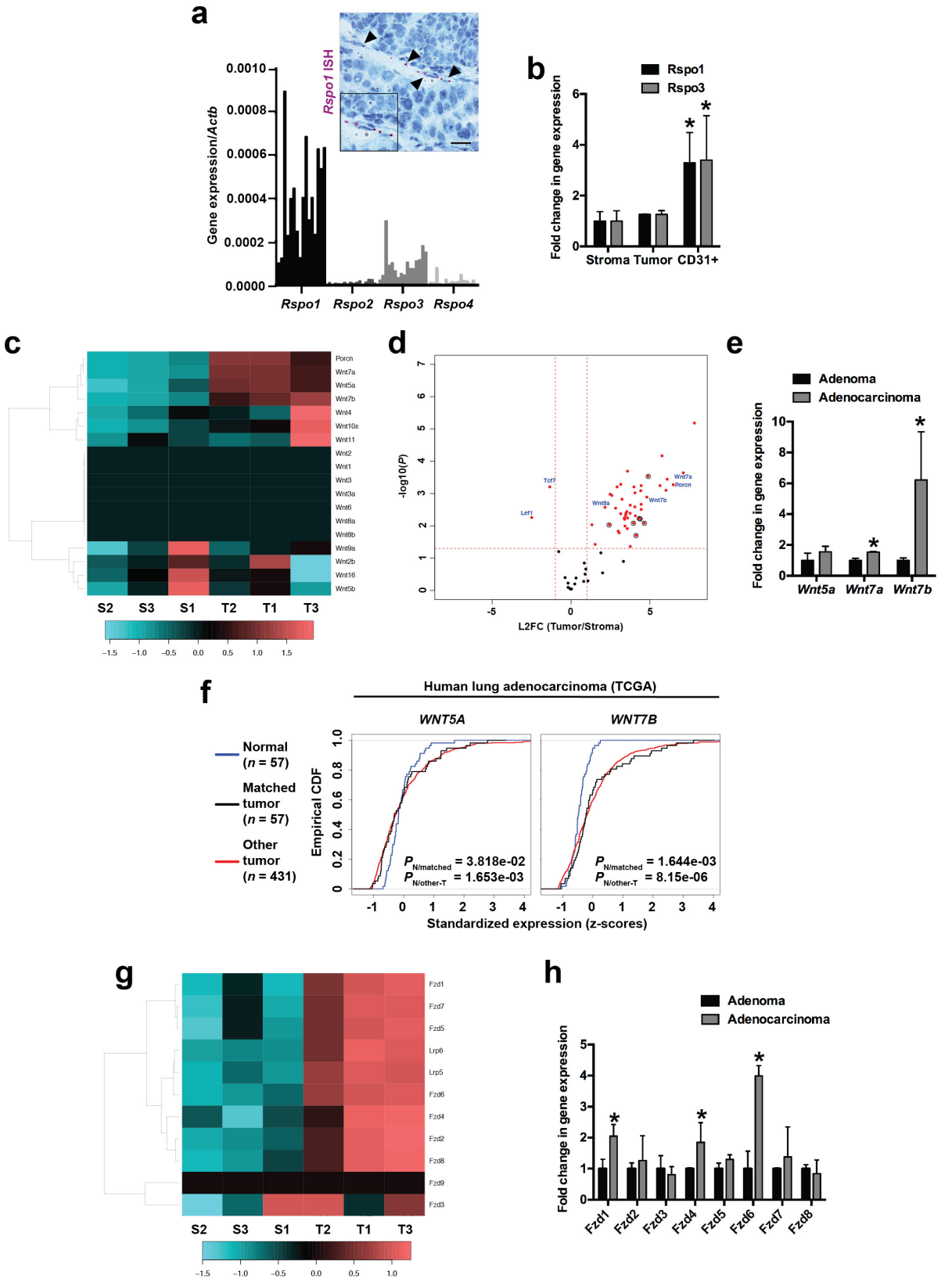

Extended Data Figure 9 | See next page for caption.

Extended Data Figure 9 | Characterization of the niche for stem-like cells in lung adenocarcinoma. a, qPCR analysis of *Rspo* gene expression in 16 KP LUAD tumours, normalized to *Actb* expression. Tumours were collected at 16 weeks after initiation with adenoviral Cre. ISH for *Rspo1* mRNA (purple, arrowheads) in a KP LUAD tumour. Note the *Rspo1* transcripts in endothelial cells. **b**, qPCR for *Rspo1* and *Rspo3* in tdTomato$^+$ tumour cells (tumour), CD31$^+$ endothelial cells and the rest of the cells (stroma) in microdissected KPT LUAD tumours following sorting. The expression of *Pecam1* (which encodes CD31) was found to be >400-fold enriched in the CD31$^+$ fraction compared to the stroma (not shown). $n = 3$ mice, representative of two replicate experiments. **c**, Heatmap showing relative expression levels of *Porcn* and the 19 mouse *Wnt* genes on the basis of the qPCR analysis in sorted tdTomato$^+$ KP LUAD cells (T) versus tdTomato$^-$ stromal cells (S) in microdissected tumours collected at 20 weeks after tumour initiation (a time point when most tumours are adenocarcinomas). **d**, Volcano plot of qPCR array gene expression analysis showing statistically significant differentially expressed genes (in red, Fzd receptors are circled). *x* axis is the $\log_2$ fold change (tumour/stroma) and *y* axis is the $-\log_{10}$ *P* value of the differential enrichment (two-sided *t*-test). **e**, qPCR analysis of *Wnt5a*, *Wnt7a* and *Wnt7b* gene expression in KP tumours microdissected at 9 weeks (adenomas) or 20 weeks (adenocarcinomas) after initiation with adenoviral Cre. $n = 6$ mice, representative of two replicate experiments. **f**, Comparison of *WNT* gene expression in tumours versus normal tissue in the TCGA lung adenocarcinoma cohort: Empirical CDF plots of standardized gene expression values for *WNT5A* and WNT7B are shown. A right-shift indicates relatively higher expression, with *P* values indicated to assess statistical significance (Kolmogorov–Smirnov test). **g**, Heatmap showing relative expression levels of *Lrp5*, *Lrp6* and nine mouse *Fzd* genes on the basis of the qPCR analysis in sorted tdTomato$^+$ KP LUAD cells (T) versus tdTomato$^-$ stromal cells (S) in microdissected tumours collected at 20 weeks after tumour initiation (a time point when most tumours are adenocarcinomas). **h**, qPCR analysis of eight *Fzd* receptors in KP tumours microdissected at 9 weeks (adenomas) or 20 weeks (adenocarcinomas) after initiation with adenoviral Cre. $n = 3$ mice. Data are mean ± s.d.; $^*P < 0.05$; Student's two-sided *t*-test (**b**, **e**, **h**).

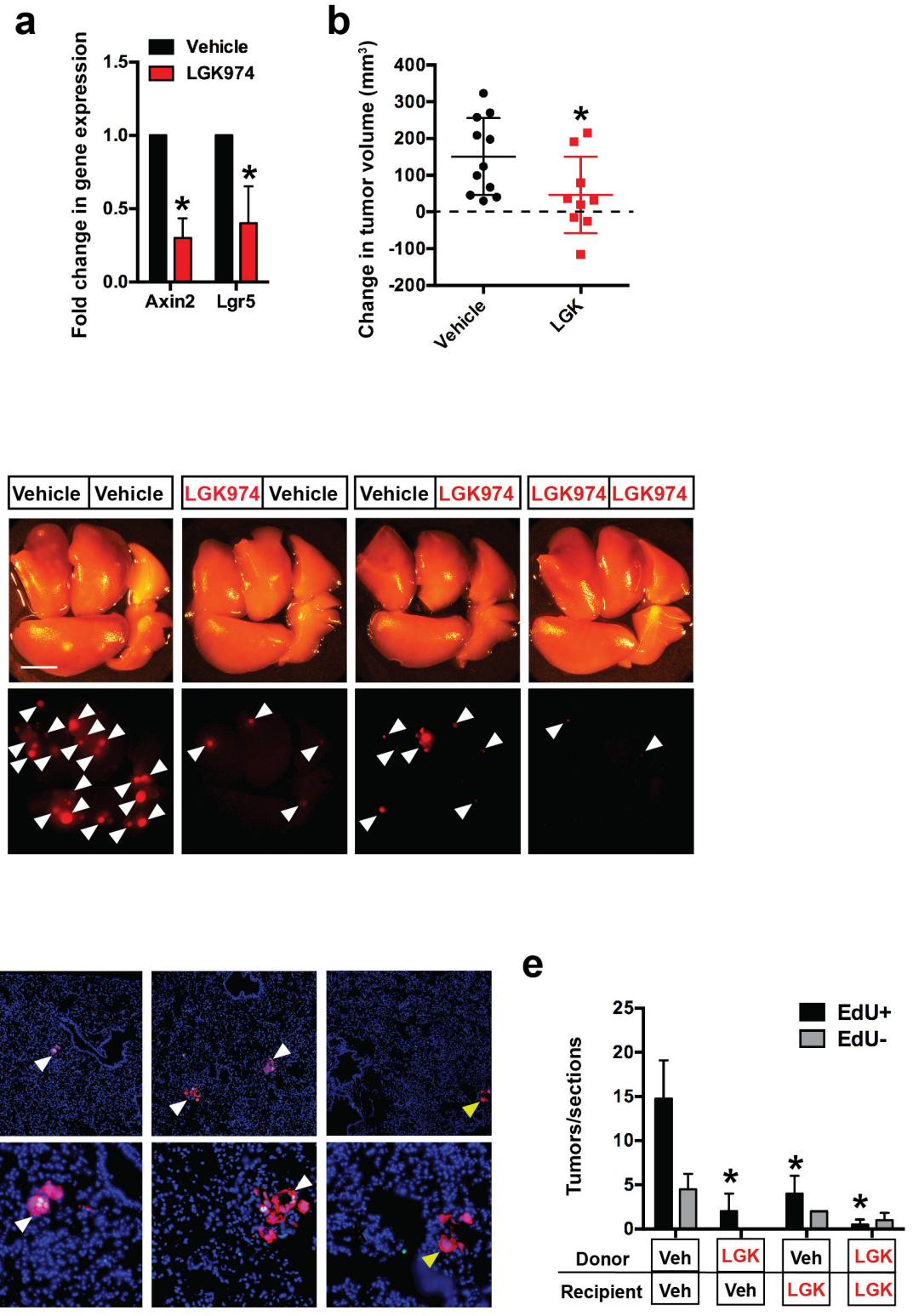

Extended Data Figure 10 | Porcupine inhibition suppresses Wnt pathway activity, progression and proliferative potential in autochthonous mouse KP lung adenocarcinomas. a, qPCR analysis of *Axin2* and *Lgr5* transcripts in KP LUAD tumours two weeks after treatment with 10 mg per kg per day LGK974 or vehicle. Treatment was started at 11 weeks after tumour initiation. $n = 6$ tumours per group. **b**, Quantification of μCT data showing change in tumour volume compared to baseline (obtained at 76 days after tumour initiation, dashed line) after four weeks of 10 mg per kg per day LGK974 or vehicle control. **c**, Recipient mouse lungs four weeks after orthotopic GEMM-DA of 50,000 primary tdTomato$^+$ (red) mouse LUAD cells. Arrowheads indicate tdTomato$^+$ tumours. Donor mice bearing autochthonous KPT LUAD tumours were treated for two weeks with LGK974 or vehicle (starting at 84 days after tumour induction). The recipient mice were treated with LGK974 or vehicle for four weeks. **d**, tdTomato$^+$ tumours in sections from lungs in **c** containing EdU$^+$ cells (white arrowheads) or not containing EdU$^+$ cells (yellow arrowheads). Scale bars, 2 mm (**c**), 500 μm (**d** (top)) and 100 μm (**d** (bottom)). **e**, Quantification of EdU$^+$ (black) or EdU$^-$ (grey) tumours per section through the lungs depicted in **c**, **d**. $n = 5$ (vehicle–vehicle), representative data from three replicate experiments. Data are mean ± s.d.; $^*P < 0.05$; Student's two-sided *t*-test (**a**, **b**) or two-way ANOVA (**e**).